

RESEARCH

Open Access



Design of a delivery vehicle chitosan-based self-assembling: controlled release, high hydrophobicity, and safe treatment of plant fungal diseases

Qing Zhou^{1†}, Zhi Xia^{1,2†}, Yu Zhang², Zhiling Sun¹, Wei Zeng¹, Nian Zhang¹, Chunmei Yuan¹, Chenyu Gong¹, Yuanxiang Zhou¹ and Wei Xue^{1*}

Abstract

Background Traditional pesticides are poorly water-soluble and suffer from low bioavailability. *N*-succinyl chitosan (NSCS) is a water-soluble chitosan derivative, has been recently used to encapsulate hydrophobic drugs to improve their bioavailability. However, it remains challenging to synthesize pesticides of a wide variety of water-soluble drugs and to scale up the production in a continuous manner.

Results A synthetic method for preparing water-soluble nanopesticides with a polymer carrier was applied. The bioactive molecule BTL-11 was loaded into hollow NSCS to promote drug delivery, improve solubility and anti-fungal activity. The synthesized nanopesticides had well controlled sizes of 606 nm and the encapsulation rate was 80%. The release kinetics, drug toxicity and drug activity were further evaluated. The inhibitory activity of nanopesticides against *Rhizoctonia solani* (*R. solani*) was tested in vivo and in vitro. In vivo against *R. solani* trials revealed that BTL-11 has excellent control efficiency for cultivated rice leaf and sheath was 79.6 and 76.5%, respectively. By contrast, for BTL-11@NSCS NPs, the anti-fungal ability was strongly released and afforded significant control efficiencies of 85.9 and 81.1%. Those effects were significantly better than that of the agricultural fungicide azoxystrobin (51.5 and 66.5%). The proposed mechanism was validated by successfully predicting the synthesis outcomes.

Conclusions This study demonstrates that NSCS is a promising biocompatible carrier, which can enhance the efficacy of pesticides, synergistically improve plant disease resistance, protect crop growth, and can be used for the delivery of more insoluble pesticides.

Highlights

- *N*-succinyl chitosan as a delivery vehicle material.
- Green, efficient, and safe BTL-11@NSCS NPs nanopesticides were prepared by utilizing NSCS in combination with the bioactive molecule BTL-11.

[†]Qing Zhou and Zhi Xia: Co-first authors.

*Correspondence:

Wei Xue

wxue@gzu.edu.cn

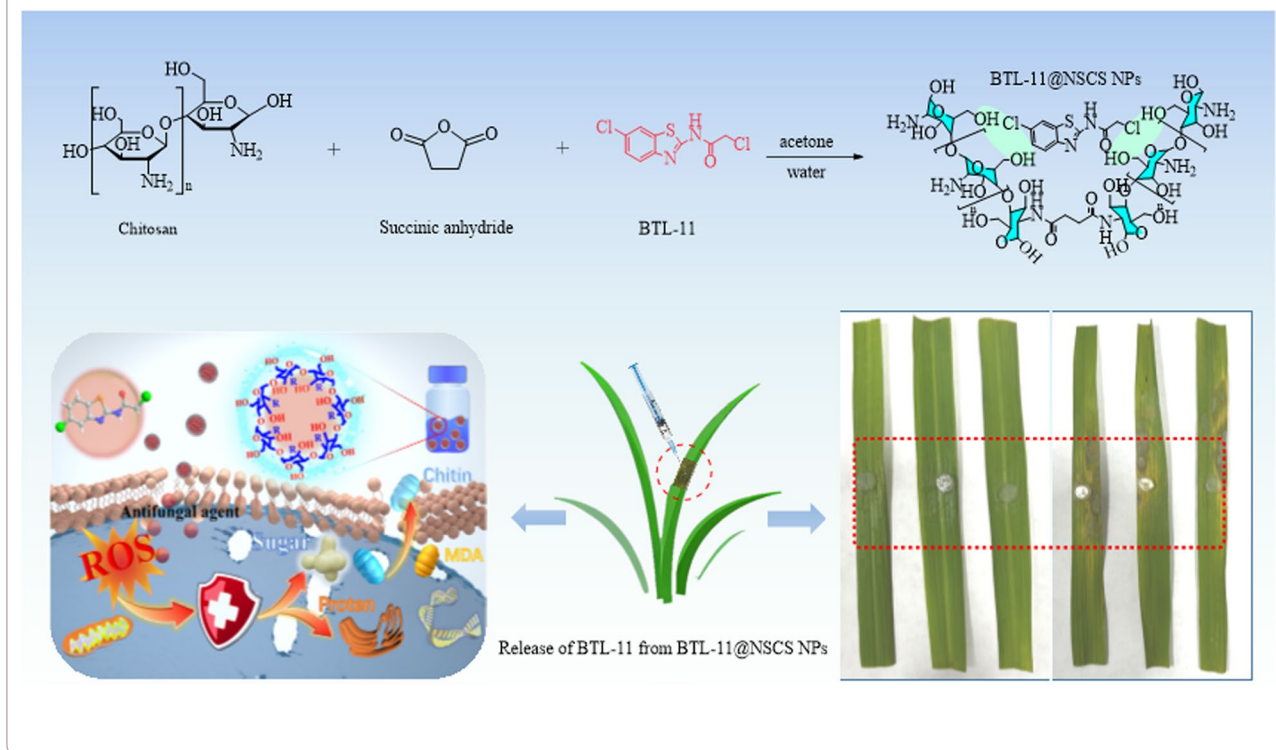
Full list of author information is available at the end of the article



- BTL-11@NSCS NPs has a small, uniform, stable morphology feature, and outstanding physicochemical properties.
- Controlled release, high hydrophobicity, and safe treatment of plant fungal diseases.

Keywords *N*-succinyl chitosan, Nanopesticide, Bioactive molecule, Anti-fungal activity

Graphical Abstract



Introduction

Rice is considered one of the most important plants globally, as it is the source of food for more than half of the world's population [1–3]. However, fungal diseases are increasingly recognized as a global threat to food security, crop destruction and forest ecosystem dynamics [4–6]. Rice plants are susceptible to rice blast, leaf blight, and stripe blight, and the occurrence of multiple rice diseases can negatively affect crop growth and lead to substantial yield loss in all rice growing regions of the world [7–9]. Since 1960s, a multitude of cost effective fungicides have been used to protect crops from fungal infections. Those played an instrumental role in dealing with the demand for food as a result of rapid population growth [10–14]. Nevertheless, owing to the excessive use of fungicides with the same or similar mode of action, fungicide resistance is rapidly increasing, which resulting in the decrease of ability to control fungal diseases in crops [15–17]. Meanwhile, non-target and environmental hazards have

emerged along with fungicide utilization [18, 19]. Therefore, it is an outstandingly meaningful project to continue to develop green, efficient, and environmentally friendly new fungicides to control fungal diseases in crops.

In recent decades, nanotechnology has been developing rapidly and widely used in many fields, and it is like a rising star for bio-agriculture, offering many strategies to address the drawbacks of traditional pesticides, agricultural design and manufacture of green pesticide formulations [20–22]. Nanopesticides is a sign of the technological development of pesticides, which has efficacy, durability, and reduces the amount of active ingredient required [23–25]. The development and characterization of green composites are based on natural fibers, especially chitosan, chitosan blends, and chitosan nanocomposites, which have attracted much attention due to their applications in the fields of bio-medicine, bio-industry, drug slow-release materials, and environmental protection [26–28]. Chitosan (CS) is an amino

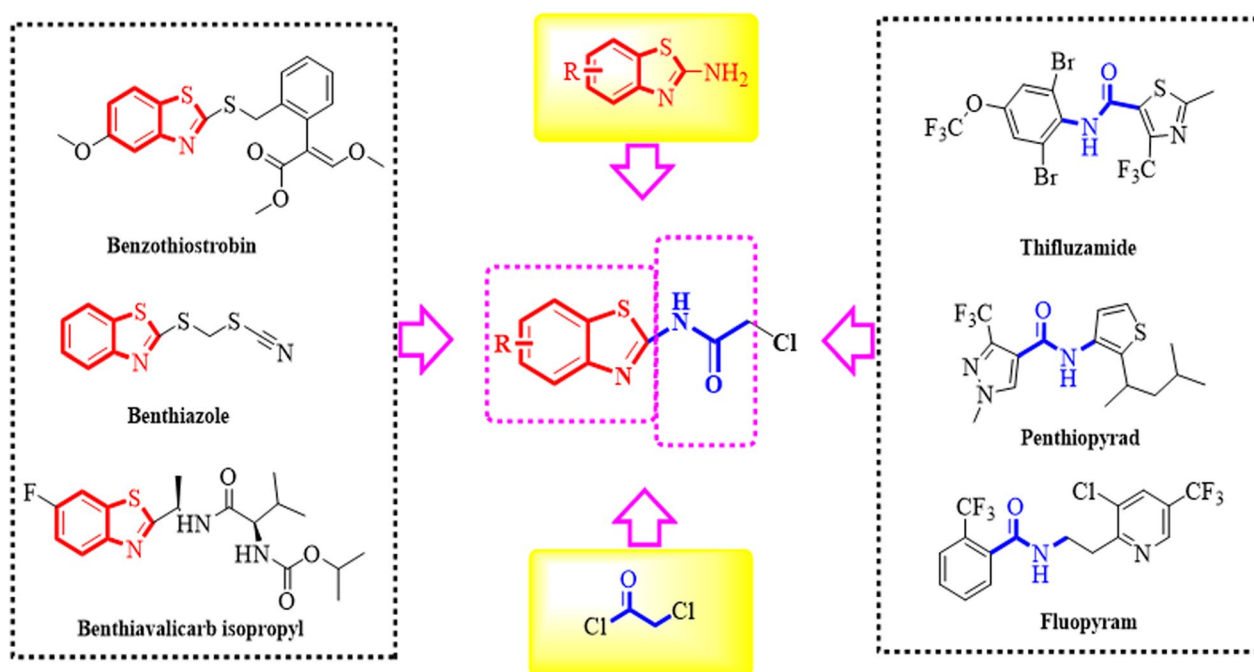


Fig. 1 Design of target compounds by using active structure splicing

polysaccharide obtained from the partial or total deacetylation of natural polymer chitin. CS has rich amine, hydroxyl and other active functional groups [29–31], which attracted significant attention due to its bio-degradability, bio-compatibility and bio-activity, and has been applied to adsorbent tablets, nanoparticles, films, hydrogels, and so on [32–35]. Although chitosan itself is insoluble in water, a variety of chitosan derivatives with different properties can generate through chemical reactions under the premise of chemical modification of chitosan, thus expanding the scope of application of chitosan [36]. Among them, the inhibitory effect of chitosan on plant fungal diseases plays a bridging role in agricultural engineering [37–39]. However, there are few studies on the use of CS as a carrier to deliver active ingredients and make value of waste material. Considering the unique properties of CS, it is hypothesized that it could interact with NSCS polymers through non-covalent molecular recognition to form an assembled system, thereby building an efficient [40–42], multifunctional and sustainable pesticide delivery platform.

The succinate dehydrogenase inhibitors (SDHI) fungicides with amide bridge has been successfully developed and commercially utilized, which exhibited significant fungicidal efficacies and low cross-resistance [43]. By using active structure splicing (Fig. 1), 24 benzothiazole amides active small molecules were synthesized. The BTL-11 possessed a wide range of anti-fungal activities, especially significant in vitro inhibitory activity against

rice blast fungus. However, since the BTL-11 is insoluble in water, it is difficult to be applied in production practice. Further, the bioactive molecule BTL-11 was encapsulated in an aqueous solution of NSCS to obtain novel BTL-11@NSCS NPs pesticides. Fourier transform infrared spectroscopy (FTIR), transmission electron microscopy (TEM), dynamic light scattering (DLS), and fluorescence spectroscopy (FS) were used to characterize the physicochemical properties of NSCS and BTL-11@NSCS NPs. Moreover, the BTL-1–BTL-24 and BTL-11@NSCS NPs complex would be evaluated with plant disease as well as in vitro and in vivo anti-fungal activities against phytopathogen *Rhizoctonia solani* (*R. solani*). Finally, the anti-fungal mechanism would be investigated from pathogen' morphological studies, fluorescent staining results, and enzyme activity test experiments. The results displayed that BTL-11@NSCS NPs could interfere with the synthesis of the cell wall of *R. solani*, destroy the cell membrane, cause the separation of the cell wall, enhance the permeability of the cell, enter the cell and act on a variety of organelles, eventually leading to serious damage to the cell structure, causing the mycelium to wilt and fold, unable to grow normally or even die.

Methods

Instruments and chemicals

The NMR data ^1H , ^{13}C , and ^{19}F of BTL-1–BTL-24 were determined on Bruker Biospin AG-400 NMR

spectrometer (Bruker Optics, Switzerland). X-ray single crystal structure data were obtained on X-ray diffractometer (Bruker, Germany). Scanning electron microscopy (SEM) data were obtained on FEI Nova Nano 450 (Hillsboro, OR, USA). FTIR data were obtained on Thermo Fisher Scientific (USA). TEM and Energy dispersive X-ray spectroscopy (EDS) data were obtained on FEI Talos F200X (USA). The critical micelle concentration (CMC) was determined by F98 fluorescence spectrophotometer (Lengguang Technology, China). Particle size distribution and zeta potential (in liquid) were determined by Zetasizer Nano ZS90 (Malvern, UK).

The chitosan (deacetylation degree >95% and viscosity of 100–200 mPa s), succinic anhydride, acetone, pyrene, ethyl alcohol, thiourea, substituted 2-chlorophenol, 2-amino-substituted benzothiazole, and ethyl acetate were purchased from Tansoole Chemicals Company (Adamas, Shanghai, China). Various assay kits were purchased from Beijing Solarbio Science & Technology Co., Ltd.

The preparation method of the target compounds BTL-1–BTL-24

A variety of substituted amines reacted with chloroacetyl chloride (at molar ratio of 1:1.2) in CH₂Cl₂ system in ice bath for 1 h to obtain corresponding benzothiazole amides [44].

Preparation of NSCS and BTL-11@NSCS NPs

CS (1.0 g) was dissolved in 200 mL of 1% acetic acid solution (in a three-neck flask) under stirring. Dissolve 0.2 g succinic anhydride in 20 mL acetone, slowly add it dropwise to the above chitosan acetic acid solution at room temperature, and then stir at 40 °C for 4 h. After cooling, add excessive acetone for precipitation. Remove solvent by vacuum suction filtration. Finally, the product was dried in vacuum at 40 °C, and the faint yellow substance obtained was NSCS. NSCS was ultrasonically dissolved in distilled water and prepared into aqueous solution (1.0 mg/mL). Next, different amounts of BTL-11 were added to the above solution to form an emulsion by ultrasonic dispersion to obtain BTL-11@NSCS nanoparticles (BTL-11@NSCS NPs) with different drug loading [45]. The synthesis principle was shown in Scheme 1.

The critical micelle concentration (CMC).

NSCS micellar water dispersions with a certain concentration were prepared. The diluted concentrations were 1.0, 0.8, 0.6, 0.4, 0.2, 10⁻¹, 10⁻², 10⁻³, 10⁻⁴, 10⁻⁵ mg/mL, and 10 μL of 0.6 μmol/L pyrene acetone solution was added respectively and it was left in a vacuum drying oven overnight at 50 °C. The fluorescence detection was carried out after pyrene molecules were stable in the system. Detection conditions of fluorescence

spectrophotometer: scanning wavelength range: 350–450 nm, excitation wavelength: 337 nm, scanning speed: 60 nm/min, excitation and emission slit width: 5.0 nm [46].

Loading content (LC) and encapsulation efficiency (EE)

BTL-11 (1.0, 2.0, and 5.0 mg) was ultrasonically dissolved in 10 mL of NSCS aqueous solution (1.0 mg/mL), respectively. Then the solution was centrifuged at high speed for 3 min, and the supernatant was taken and filtered through a filter membrane with 0.22 μm pore size. The amount of BTL-11 entrapped or adsorbed in the NSCS NPs was determined by HPLC. The operating conditions for HPLC determination were as follows: Agilent XDB-C18 reverse phase column (5 mm, 4.6 × 250 mm), column temperature (30 °C), acetonitrile and aqueous solution (V/V=60:40) were used as mobile phase with a flow rate of 1.0 mL/min. The detection wavelength was set at 310 nm and the injection volume was 5 μL.

Drug release and phytotoxicity tests

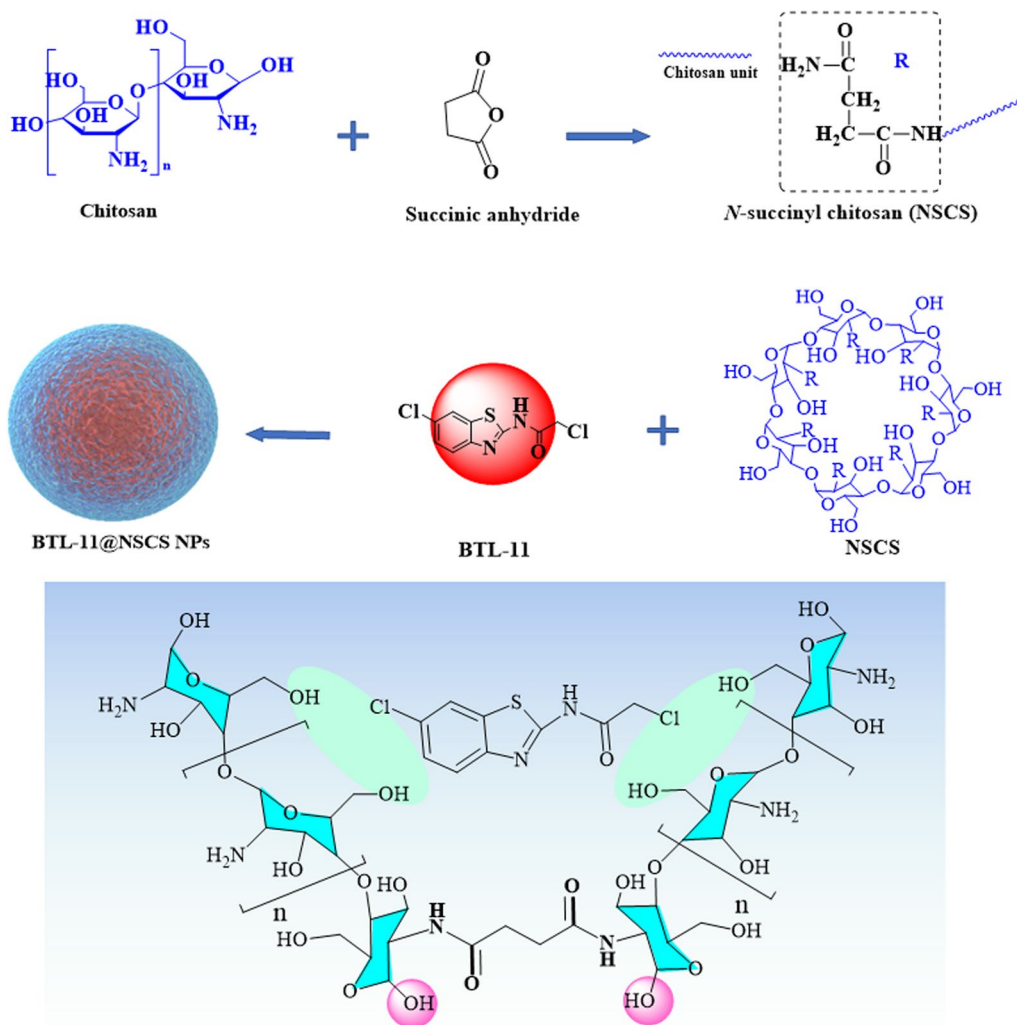
The influence of pH on NPs and especially on nanocapsules is significant factor [47, 48]. The mixture of NSCS and BTL-11 (NSCS:BTL-11=2:1) was ultrasonically dispersed in 50 mL distilled water. Five different pH values of 5.0, 6.0, 7.0, 8.0 and 9.0 were set to investigate the relationship between pH value and release behavior. These solutions were shaken in a constant temperature shaker (Shanghai Yiheng Scientific Instrument Co., Ltd., Shanghai, China) with a speed of 200 rpm at 30 °C. The released solution of 3 mL was withdrawn at different time intervals for analysis. To keep the total solution volume as constant, an equal volume of phosphate buffer solution (PBS) with different pH values (3 mL) was further added. The concentration of BTL-11 in the solution was determined by UV spectrometry (209 nm). The accumulative BTL-11 released was calculated according to the following equation [49, 50].

$$\text{Release (\%)} = \frac{V_0 \times C_t + V \times \sum_{n=1}^{t-1} C}{W}$$

where Release is the accumulative release of BTL-11 from the hydrogels; V_0 is the volume of the released medium (50 mL); C_t is the concentration (mg/mL) of BTL-11 in the release medium at sampling time; V is the volume of each sampling (3 mL); W is the total quantity (mg) of BTL-11 entrapped in the NSCS hydrogels.

In vitro and in vivo of target compounds against *R. solani*, *P. capsici*, *B. cinerea*, and *S. sclerotiorum*

The assessed effects of the BTL-1–BTL-24 on the mycelial growth against *Rhizoctonia solani* (*R. solani*),



Scheme 1 Schematic diagram of the synthesis principle of BTL-11@NSCS NPs based CS

Sclerotinia sclerotiorum (*S. sclerotiorum*), *Botrytis cinerea* (*B. cinerea*), and *Phytophthora capsici* (*P. capsici*) [51, 52].

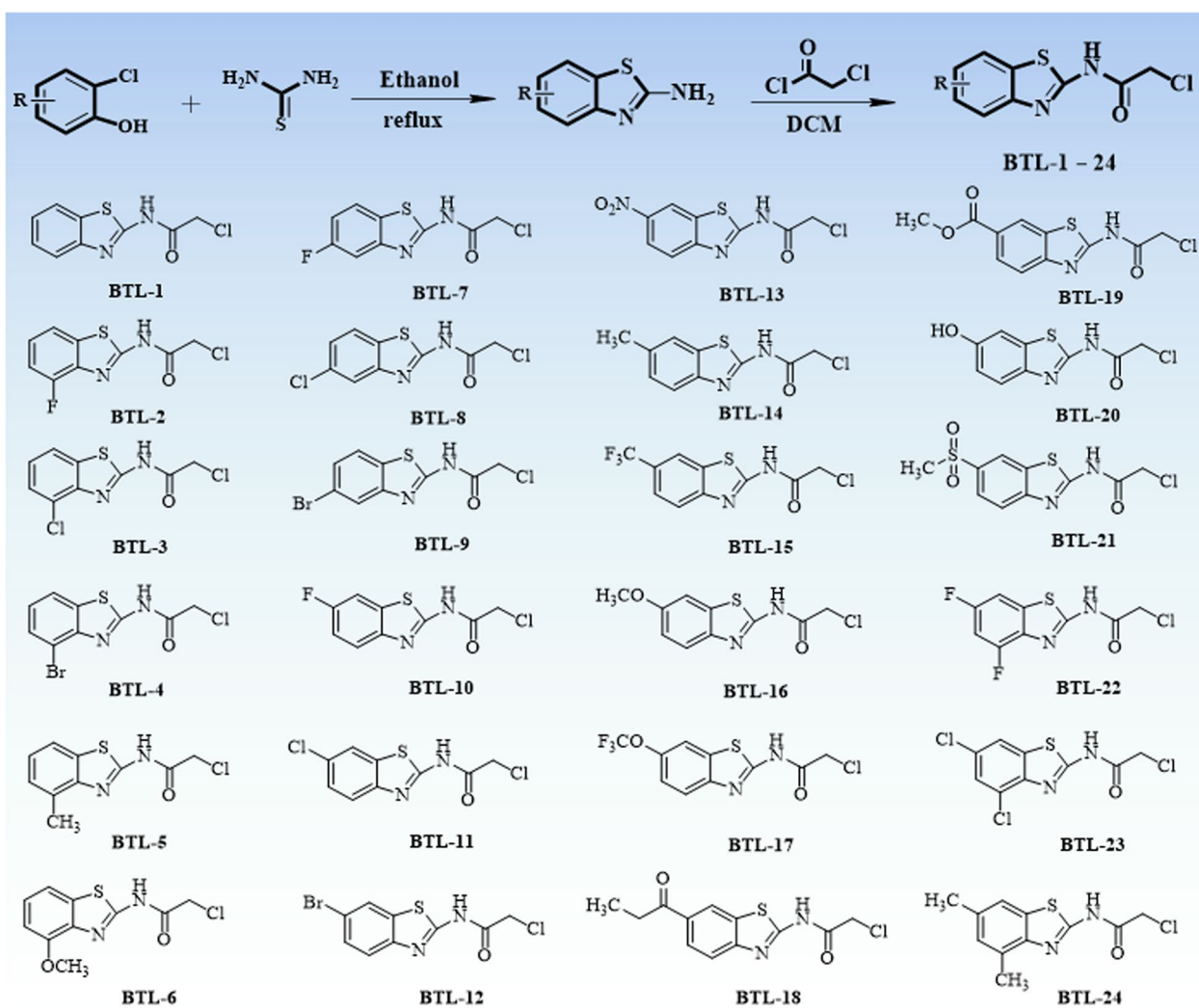
In vivo protective activity against *R. solani* had been explored. In order to evaluate the protective activity against rice sheath blight, the rice plants were inoculated with *R. solani*, which were treated of target compound solution, and azoxystrobin was used as a positive control [53, 54]. Each was treated with 12 plants, after 72 h the control effect is calculated by the formula:

$$\text{Inhibition ratio (\%)} = \frac{C - T}{C} \times 100$$

C is the diameters of the lesion without treatment; T is the diameters of the lesion with treatment.

Sclerotia formation and germination inhibiting tests

The mycelial disks (5 mm) of *R. solani* were inoculated into potato dextrose agar (PDA) containing (50, 25, 12.5, 6.25, 3.125, and 0 $\mu\text{g/mL}$) of BTL-11 and BTL-11@NSCS NPs and cultured at 28 °C in the dark for 21 d. The formed sclerotia were collected and dried at 60 °C for 24 h, and the number and weight of the sclerotia were calculated. *R. solani* were cultured for 21 d to obtain sclerotia. Different concentrations (50, 25, 12.5, 6.25, 3.125, and 0 $\mu\text{g/mL}$) of BTL-11 and BTL-11@NSCS NPs were prepared and then 5 sclerotia were placed on the culture, and each concentration consisted of three replicates. These dishes were incubated at 28 °C for 32 h, and then the inhibition rate of the compounds on the germination of sclerotia was calculated [55].



Scheme 2 The synthetic route and structure of target molecules BTL-1–BTL-24

Effect on *R. solani* morphology

The references describe detailed procedures for Light microscopy (LM), Fluorescence microscope (FM), and SEM measurements [56].

Effects on the growth and respiratory energy metabolism, cell wall, and membrane permeability of *R. solani*

Chitinase, malondialdehyde (MDA), protein, and total sugar content were tested by Refs. [57–60].

Molecular docking

The three-dimensional structures of BTL-11, fluopyram, and oxidoreductase (PDB code: 2FBW) were further treated by Discovery Studio 2019 Client to generate the docking input files and finish molecular docking studies.

The obtained three-dimensional binding modes of bioactive molecules with oxidoreductase were shown by Discovery Studio 2019 Client to gain the corresponding two-dimensional binding modes [61].

Results and discussion

Characterization of target compounds BTL-1–BTL-24, NSCS, and BTL-11@NSCS NPs

As shown in Scheme 2, 24 benzothiazole amides derivatives were summarized. The NMR and cultured X-ray single crystal structure data (BTL-8: Additional file 1: Table S7 and Additional file 1: Fig. S3) of the target compounds were provided in Additional file 1.

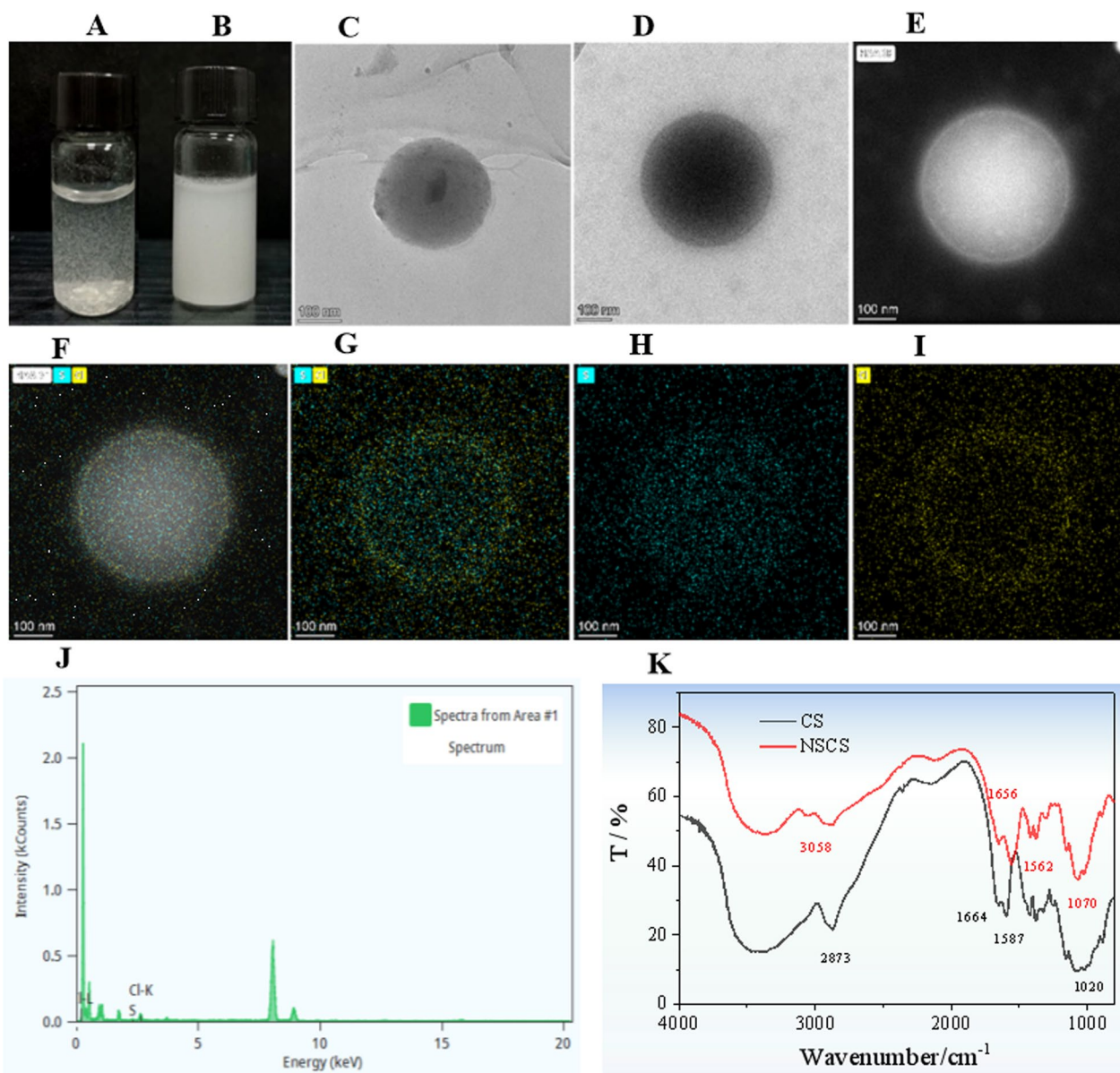


Fig. 2 Photographs of solutions of BTL-11 and BTL-11@NSCS NPs 2 mg/mL in water (A) and NSCS aqueous solution (B); TEM images of NSCS (C) and BTL-11@NSCS NPs (D, E); Elemental mapping (F–I) and EDS (J) of BTL-11@NSCS NPs; FTIR spectra (K) of CS and NSCS

The photographs of solutions of BTL-11 and BTL-11@NSCS NPs 2 mg/mL in water were shown in Fig. 2A. It could be seen from the figure that BTL-11 was in suspension in water, mainly because of its poor water solubility. When it was added to NSCS aqueous solution, it was in white emulsion state, and the dispersion was significantly enhanced (Fig. 2B).

The morphology of the prepared NSCS colloid and BTL-11@NSCS NPs were characterized on TEM. The NSCS colloid exhibited a spherical shape without adsorption or adhesion, and have essentially the same

color from the center to the periphery (Fig. 2C). This result indicated that NSCS can self-assemble in distilled water. The spherical color of BTL-11@NSCS NPs was darker, clearer, and more uniform than that of NSCS. This attributed to the fact that BTL-11 contains chlorine, sulfur elements, and has a higher density (Fig. 2D, E). The experiments revealed that BTL-11 could induce NSCS to package and assemble into spherical nanoparticles faster and better. The elemental mapping images of BTL-11@NSCS NPs (Fig. 2F–I) displayed the homogeneous spatial distribution of chlorine and sulphur

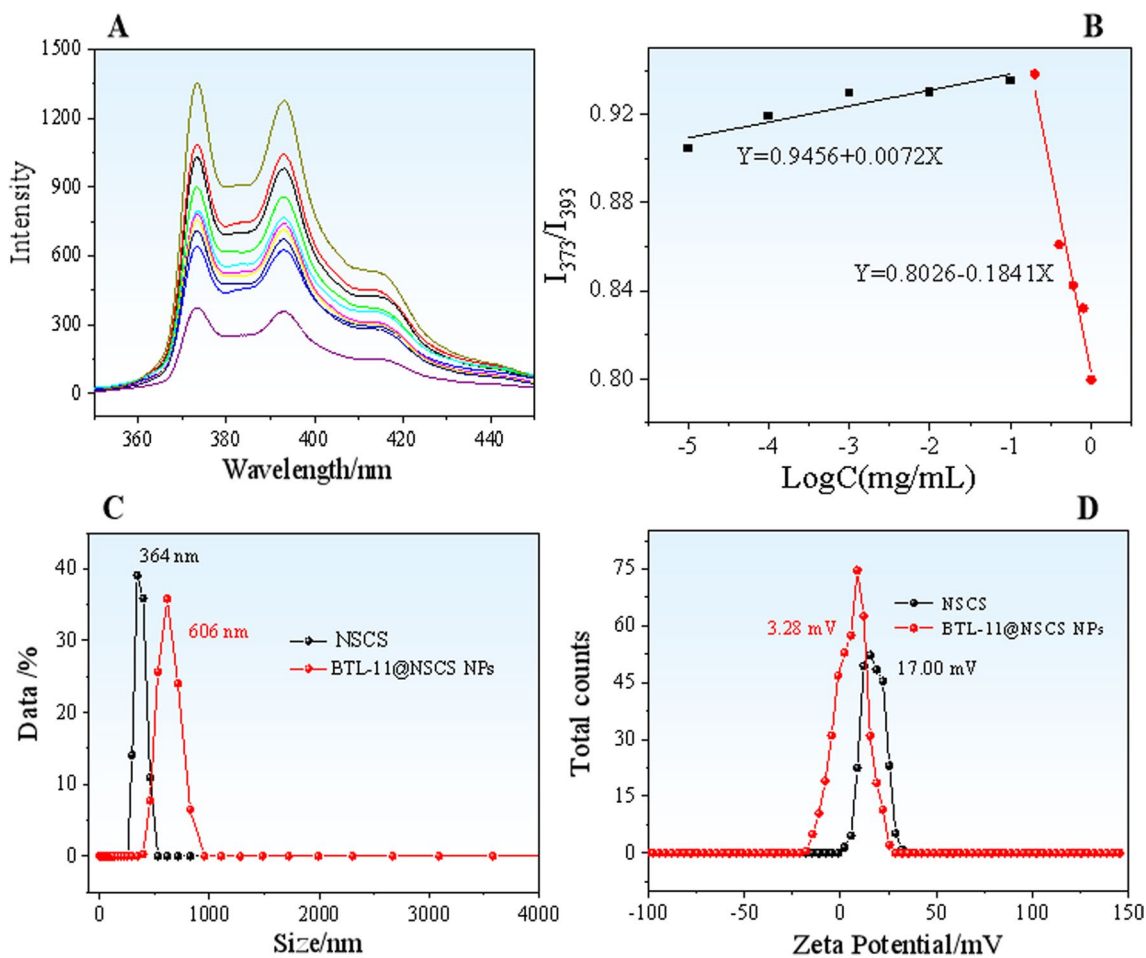


Fig. 3 The fluorescence spectra of pyrene in aqueous NSCS solutions with different concentrations from 10 mg/mL to 1.0 mg/mL (A); The relationship between logarithm of concentration and peak ratio (B). Size distribution (C) and zeta potential (D) of NSCS and BTL-11@NSCS NPs (in liquid)

elements on the BTL-11@NSCS NPs. The EDS measurement further proved the existence of chlorine and sulphur atoms (Fig. 2J).

The FTIR spectrums of NSCS and CS (Fig. 2K) were recorded on KBr pellet method [62]. The absorption bands of $-\text{OH}$ and $-\text{NH}_2$ in the CS at $3310\text{--}3500\text{ cm}^{-1}$ were narrowed after the succinylation reaction. 3058 cm^{-1} was the absorption band of $-\text{NH}$, which indicated that the CS was scandalized. 1020 and 1070 cm^{-1} were the absorption bands of the primary hydroxyl and secondary hydroxyl, which changed very little before and after the reaction, respectively. The absorption band at 1857 cm^{-1} disappeared after succinylation, and the amide I band at 1656 cm^{-1} and amide II band at 1562 cm^{-1} appeared in the CS, which further confirmed the formation of $-\text{NH}-\text{CO}-$ structure in the chitosan molecule.

Critical micelle concentration (CMC) of NSCS

CMC is the lowest concentration of surfactant in water or other solvents to form micelles [63]. In this study, pyrene was used as a fluorescent probe to detect the CMC value of NSCS. The solubility of pyrene in water was very low. Amphiphilic copolymer NSCS had solubilizing effect on nonpolar organic compounds. With the continuous change of concentration gradient, the solubilizing ability of the copolymer NSCS to pyrene changes constantly. When the polymer forms micelles in water, pyrene could quickly transfer from the hydrophilic environment to the hydrophobic core of the micelles, resulting in the change of fluorescence absorption [64]. When the copolymer concentration increased to a certain value, the fluorescence peak ratio changed sharply, which proved the formation of copolymer micelles. The smaller the CMC

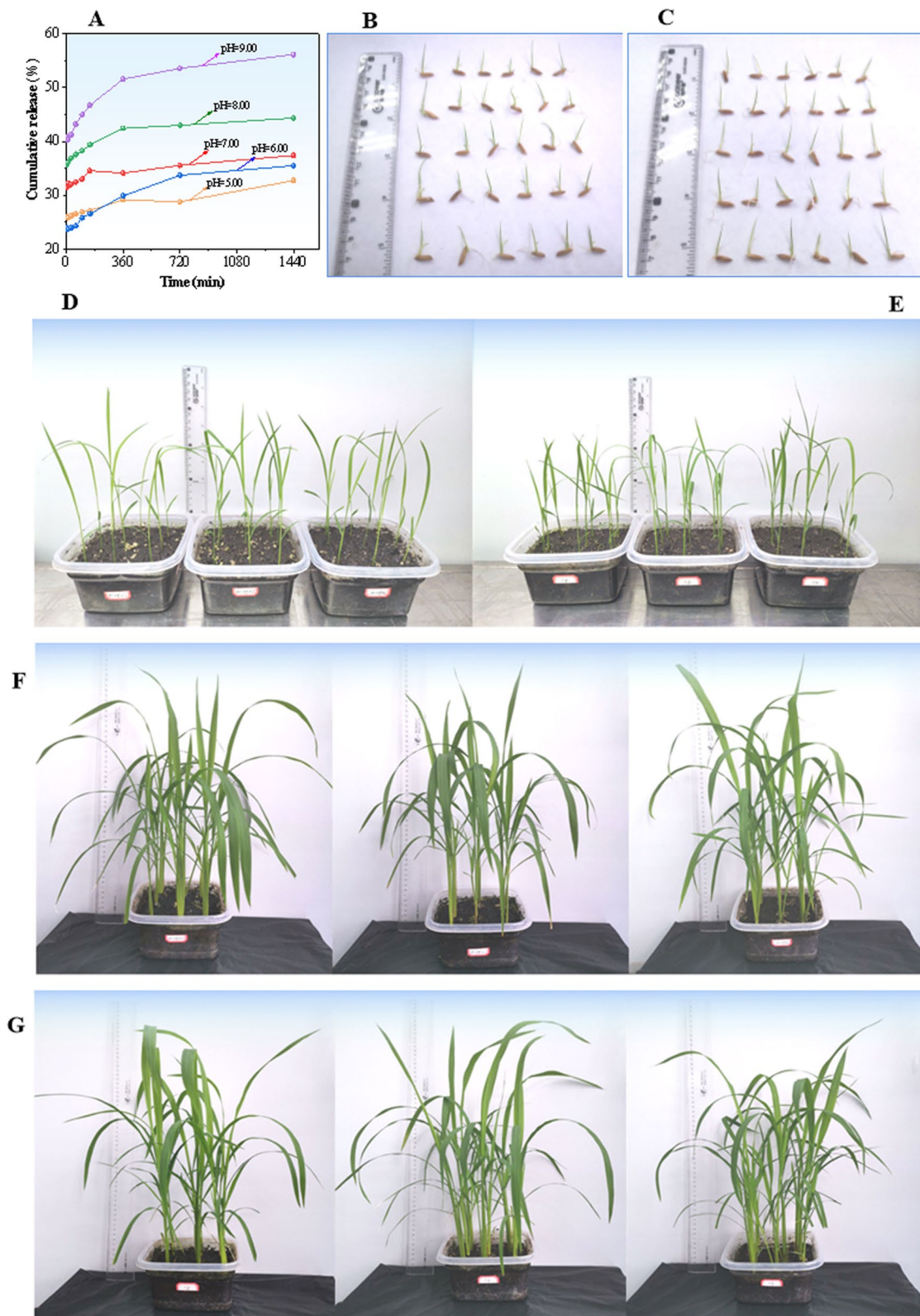


Fig. 4 Cumulative release of BTL-11 from BTL-11@NSCS at different pH values (**A**); Phytotoxicity studies after the spraying of BTL-11@NSCS NPs; **B**, **D**, and **F** are after spraying of BTL-11@NSCS NPs, the rice plants were cultured for different periods; **C**, **E**, and **G** is the blank groups without drugs

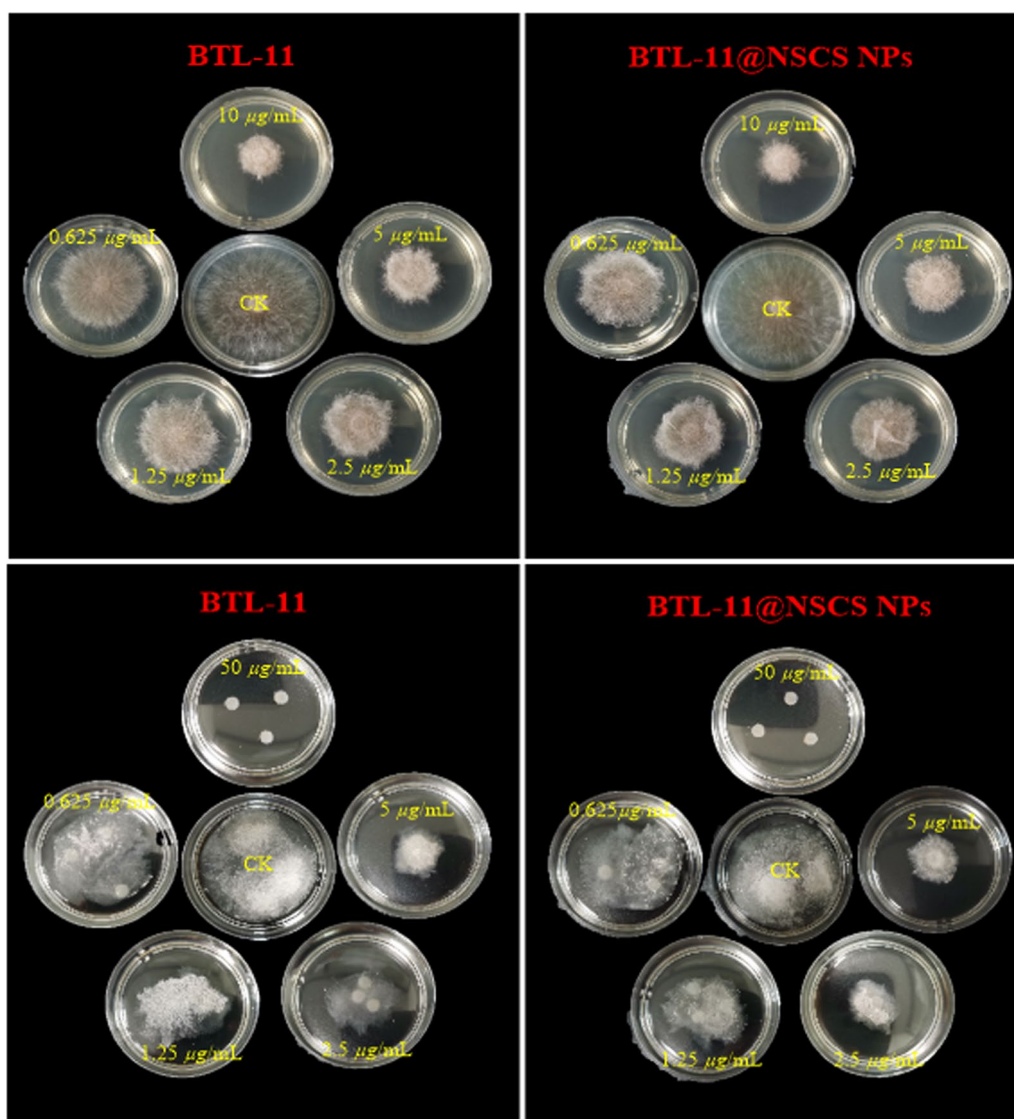


Fig. 5 Anti-fungal effects of BTL-11 and BTL-11@NSCS NPs on *R. solani* under different media conditions

value, the more stable the polymer was in aqueous solution [65]. Figure 3A showed the fluorescence spectra of pyrene with the same concentration in different concentrations of NSCS. The illustration demonstrated the relationship between the ratio of the fluorescence intensity of the first and third vibrational bands (I_{373}/I_{393}) in the pyrene emission spectrum and the concentration of NSCS. The curve showed that the ratio of I_{373}/I_{393} increased slowly at first, and then decreased sharply (Fig. 3B). The CMC of NSCS in water was determined to be 0.1788 mg/mL.

Particle size and zeta-potential analyses

The particle size of nanoparticles in aqueous solutions was analyzed by using dynamic light scattering technology, the particle size distribution curve was shown in Fig. 3C. The particle size range of NSCS was from 255 to 450 nm, with an average particle size of 364 nm. The particle size range of BTL-11@NSCS NPs was from 390 to 1000 nm, with an average particle size of 606 nm. Compared with NSCS, the nanoparticle distribution of BTL-11@NSCS NPs has widened, and the average particle size

Table 1 The EC₅₀ values of target compounds against *R. solani*^A

Compounds	R	Regression equation	r ²	EC ₅₀ (µg/mL)
BTL-1	H	y = 1.4403x + 3.3581	0.9932	13.8 ij
BTL-2	4-F	y = 1.2104x + 3.6327	0.9630	13.4 j
BTL-3	4-Cl	y = 1.3063x + 3.8144	0.9856	7.3 p
BTL-4	4-Br	y = 1.2214x + 3.6116	0.9832	13.7 ij
BTL-5	4-CH ₃	y = 1.1803x + 3.2980	0.9966	27.6 e
BTL-6	4-OCH ₃	y = 0.9718x + 3.7821	0.9646	17.9 h
BTL-7	5-F	y = 2.4766x + 3.9060	0.9951	2.7 r
BTL-8	5-Cl	y = 2.7841x + 2.6106	0.9671	7.2 p
BTL-9	5-Br	y = 1.3326x + 3.8441	0.9921	9.8 n
BTL-10	6-F	y = 1.1538x + 3.7625	0.9981	11.8 k,l
BTL-11	6-Cl	y = 0.7749x + 4.8997	0.9869	1.3 s
BTL-11@NSCS NPs	–	y = 0.4459x + 5.0719	0.9982	0.7 s
BTL-12	6-Br	y = 1.4780x + 3.6367	0.9801	8.3 o
BTL-13	6-NO ₂	y = 1.1031x + 3.5184	0.9849	22.0 g
BTL-14	6-CH ₃	y = 1.2208x + 3.6662	0.9966	12.3 k
BTL-15	6-CF ₃	y = 1.1606x + 3.8543	0.9940	9.7 n
BTL-16	6-OCH ₃	y = 0.9079x + 3.6190	0.9944	33.1 d
BTL-17	6-OCF ₃	y = 1.4334x + 3.5432	0.9527	10.3 m,n
BTL-18	6-COCH ₂ CH ₃	y = 1.0012x + 3.5904	0.9657	25.5 f
BTL-19	6-COOCH ₃	y = 1.2274x + 3.2635	0.9671	25.9 f
BTL-20	6-OH	–	–	> 100 a
BTL-21	6-SOOCH ₃	y = 1.0350 x + 3.8088	0.9655	14.1 i
BTL-22	4,6-di-F	y = 0.8438x + 4.3754	0.9728	5.4 q
BTL-23	4,6-di-Cl	y = 2.4080x + 4.0733	0.9813	2.4 r
BTL-24	4,6-di-CH ₃	y = 0.7123x + 3.6862	0.9950	69.9 c
Fluopyram	–	y = 1.4736x + 2.1763	0.9508	82.4 b
Azoxystrobin	–	y = 0.7673x + 4.1994	0.9735	11.1 l,m

^A The experiments were repeated 3 times, $P < 0.05$

was also much larger, mainly due to the adsorption and embedding of BTL-11 in NSCS.

The zeta potential curves of NSCS and BTL-11@NSCS NPs were exhibited in Fig. 3D. It can be seen that the potentials of NSCS and BTL-11@NSCS NPs were 3.28 and 17.00 mV, respectively, indicated that both surfaces carry positive charges. This was mainly the result of NH₂ ionization of CS, which was consistent with literature reports. These positively charged nanoparticles on the surface were conducive to the stable existence of nanoparticles over a longer period of time due to electrostatic repulsion. These positively charged nanoparticles on the surface were conducive to the stable existence of nanoparticles over a longer period of time due to electrostatic repulsion.

Studies of loading content (LC) and encapsulation efficiency (EE)

LC and EE are two important indicators to evaluate the pesticide loading ability of the delivery system. In this study, the peak area was used for linear regression of pesticide concentration. The results showed that under this chromatographic condition, the linear relationship was good in the range of 0.002–0.2 mg/mL, and the LC and EE were shown in Additional file 1: Table S1. It was obvious that LC and EE increase with the decrease of the ratio of NSCS to BTL-11, and EE was better. However, compared with EE, the increase of LC was more obvious. This was mainly because there were many hydrophilic segments on the surface of NSCS, which could generate

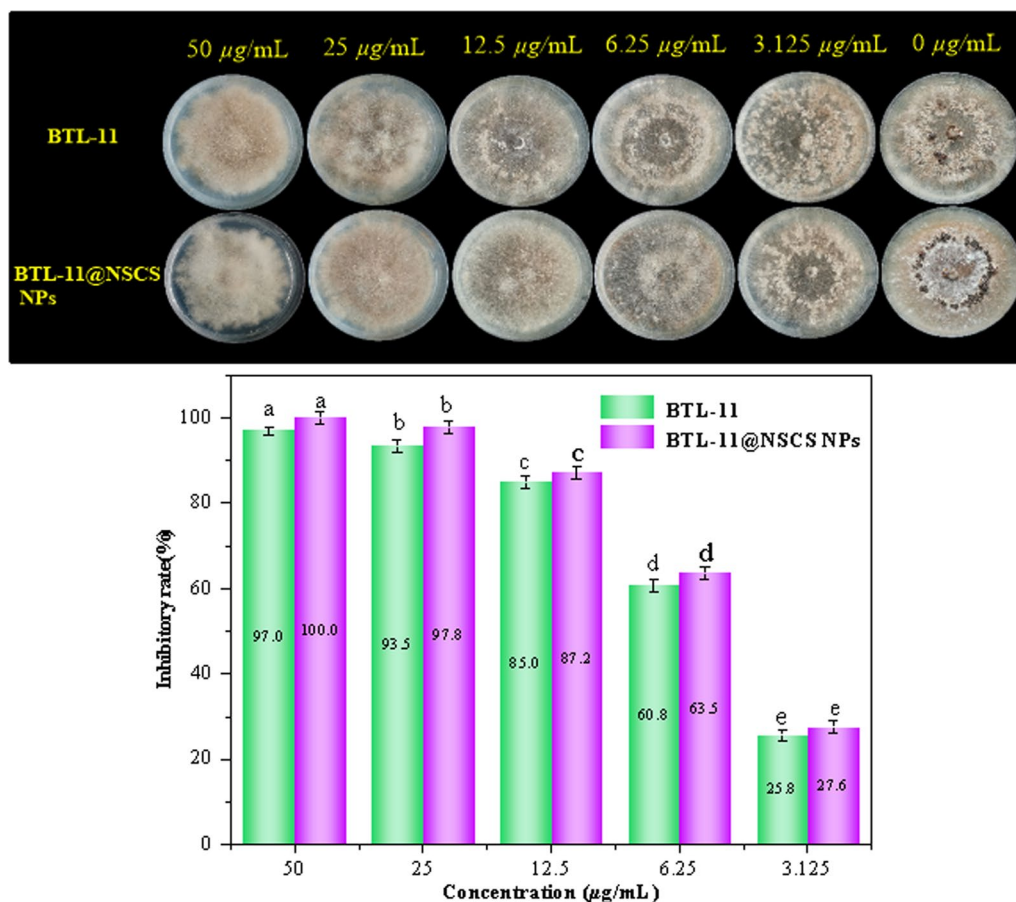


Fig. 6 Inhibitory activity of BTL-11 and BTL-11@NSCS NPs on the formation of sclerotia of *R. solani*

hydrogen bonds with BTL-11. In this way, BTL-11 will not only be embedded in the hydrophobic interior of NSCS, but also be dispersed on the surface of nanoparticles, and BTL-11 molecules will also be bound in its hydrophilic molecular chain. These results clearly illustrated the successful surface decoration of NSCS in BTL-11 and that NSCS does not impact drug loading of the final formulation.

Drug controlled release and phytotoxicity tests

In vitro drug release was studied for BTL-11@NSCS NPs by using the ultraviolet spectrophotometry. The release profiles as a function of time from the different formulations were shown in Fig. 4A. As expected, BTL-11@NSCS NPs showed rapid release over the initial 360 min followed by a slower release. The BTL-11@NSCS NPs released 44% of BTL-11 in the 1440 min at pH=8.0 (Fig. 4A). The BTL-11@NSCS NPs released 56% of BTL-11 content over a period of 1440 min with 45% of the

release occurring within the first 100 min at pH=9.0 (Fig. 4A). This may be due to the significant influence of pH on nanoparticles. The effect phytotoxicity of BTL-11@NSCS NPs on rice can be clearly seen from Fig. 4. Interestingly, rice sprouts uniformly and seedlings grow vigorously after uniform spraying of BTL-11@NSCS NPs with concentration of 500 µg/mL, the potential phytotoxicity was not observed (Fig. 4B, D). Also, the repeated spraying operations for BTL-11@NSCS NPs could not contribute to the possible phytotoxicity (Fig. 4F), confirming that the designed nanoagricultural complex was safe during application.

Biological assay against phytopathogenic fungi

Preliminary bioassay results (Additional file 1: Table S2) revealed that most target compounds exhibited pretty good anti-fungal activities against *R. solani*, *Phytophthora capsici* (*P. capsici*), *Botrytis cinerea* (*B. cinerea*),

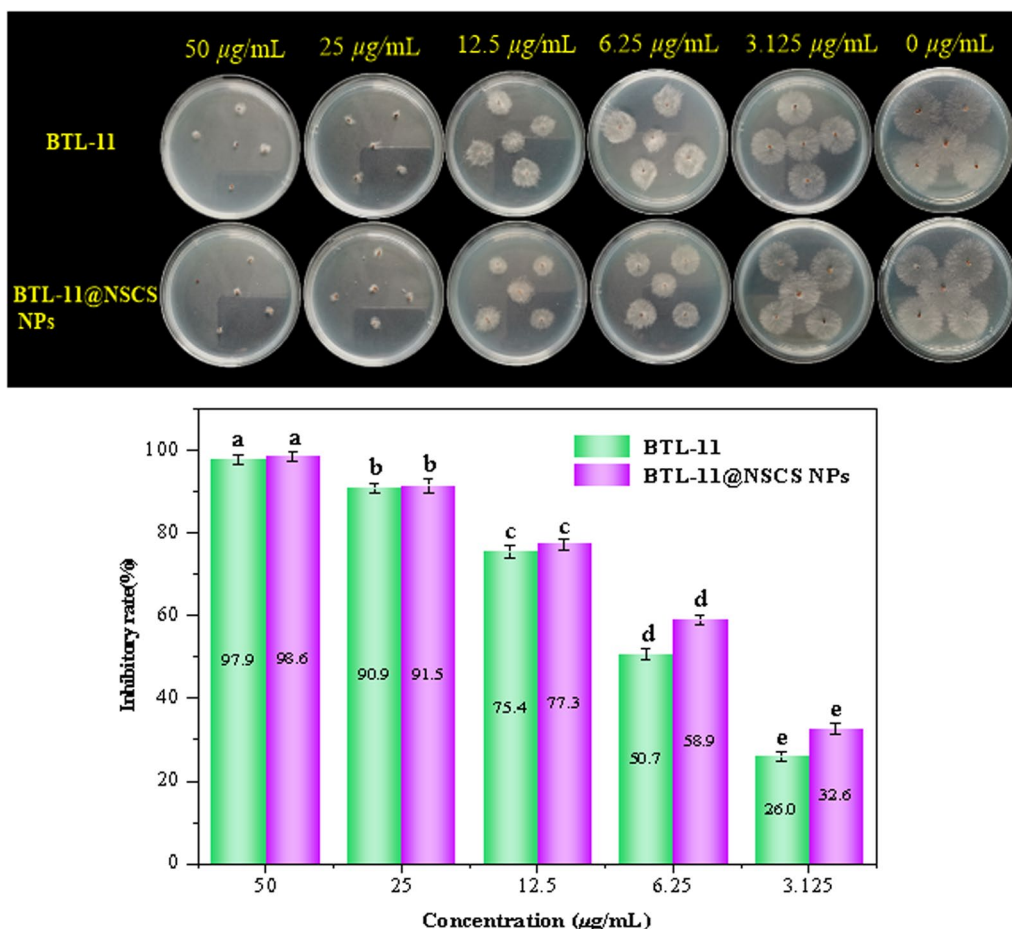


Fig. 7 Inhibitory activity of BTL-11 and BTL-11@NSCS NPs on lycopene sclerotic germination. of *R. solani*

and *Sclerotinia sclerotiorum* (*S. sclerotiorum*). Significantly, BTL-11 showed the most prominent inhibitory activity against *R. solani* (Fig. 5) compared with *P. capsici*, *B. cinerea*, and *S. sclerotiorum* at 10 µg/mL. Consequently, the half maximal effective concentration (EC₅₀) values of the target compounds against *R. solani* was further assessed by using serial dilution. As depicted in Table 1, it can be clearly visualized that the activity of BTL-11@NSCS NPs (EC₅₀=0.7 µg/mL) was significantly improved, which was better than that of the agricultural fungicide azoxystrobin (EC₅₀=11.1 µg/mL). It was therefore extrapolated that BTL-11@NSCS NPs can activate or increase the anti-fungal activity.

Inhibition of sclerotinia formation and germination

The effect on the sclerotinia formation and germination of *R. solani* were presented in Figs. 6 and 7. BTL-11@NSCS NPs showed excellent inhibitory effect on sclerotia

formation of *R. solani* were 100.0 and 27.6% at 50 and 3.125 µg/mL. However, the BTL-11 showed a poor activity at the same concentration, and the values were 97.0 and 25.8%, respectively. Moreover, BTL-11@NSCS NPs effectively inhibited the germination of sclerotia were 98.6 and 32.6% at 50 and 3.125 µg/mL, which greatly exceeded the inhibitory activity of BTL-11 on germination of sclerotia. The above experimental testes displayed that BTL-11@NSCS NPs could effectively inhibit, reduce, and spread the sclerotia formation and germination of *R. solani* infection.

Morphological testing of *R. solani*

The changes of BTL-11 and BTL-11@NSCS NPs on the mycelic morphology of *R. solani* was examined on LM (Additional file 1: Fig. S1) and SEM (Fig. 8). Control check (CK) hyphae of *R. solani* (Additional file 1: Fig. S1 A-1, A-2; Fig. 8 A1, A2) were well grown, elongated,

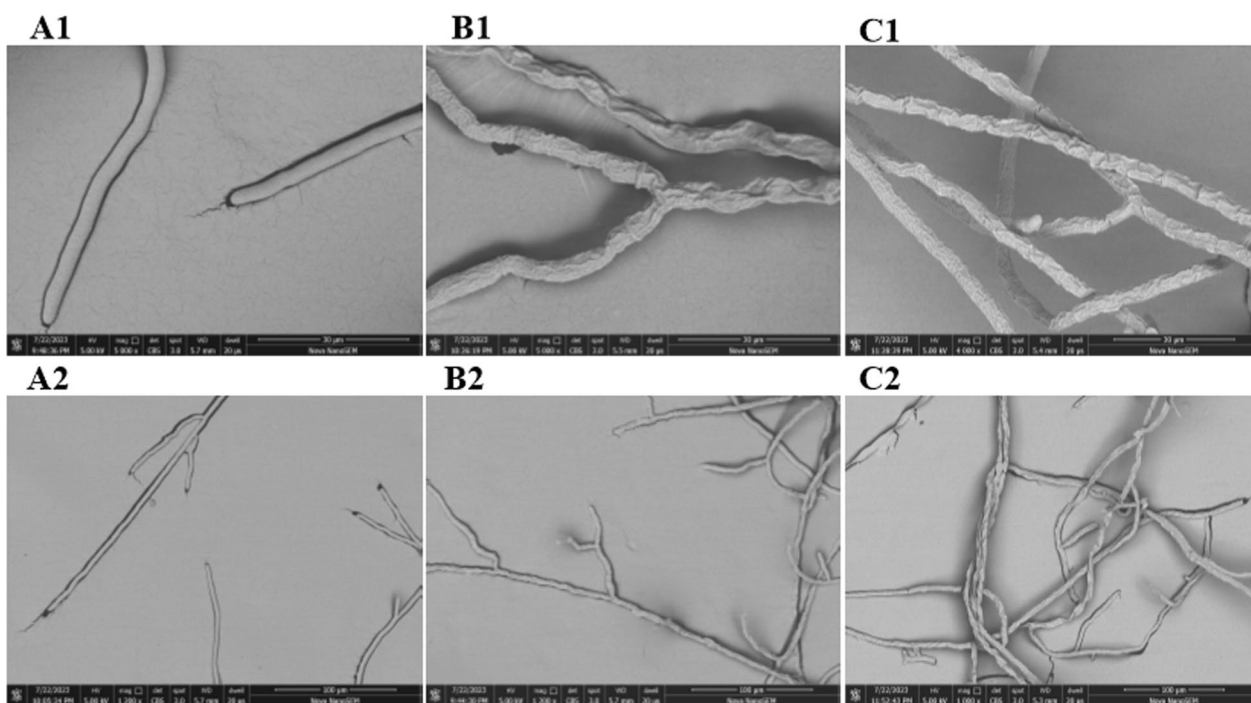


Fig. 8 The morphological changes of *R. solani* under SEM (after 12 h). **A1, A2:** CK (0 $\mu\text{g}/\text{mL}$), **B1, B2:** BTL-11 (20 $\mu\text{g}/\text{mL}$); **B2:** BTL-11 (5 $\mu\text{g}/\text{mL}$); **C1:** BTL-11@NSCS NPs (20 $\mu\text{g}/\text{mL}$); **C2:** BTL-11@NSCS NPs (5 $\mu\text{g}/\text{mL}$); scale for 30 and 100 μm

homogeneous, and well aligned. With BTL-11 (Additional file 1: Fig. S1 B-1, B-2; Fig. 8 B1, B2) and BTL-11@NSCS NPs (Additional file 1: Fig. S1 C-1, C-2; Fig. 8 C1, C2) treatment, there were an increased number of hyphal branches, short, thick, and the appearance of dry folds or even ulcers, respectively. Briefly, those finding suggested that BTL-11 and BTL-11@NSCS NPs may interfere with cell wall synthesis of *R. solani*, leading to severe disruption of the cell membrane structure.

Disruption of the *R. solani* cell wall

The Additional file 1: Table S3 and Fig. 9A revealed that the content of chitinase decreased when the concentration increased, which displayed that the compounds at high concentration hindered the normal development of the mycelium of *R. solani* and impeded mycelial growth. Moreover, the content of chitinase for BTL-11@NSCS NPs was 125.4 U/g at 100 $\mu\text{g}/\text{mL}$, which was much lower than that of BTL-11 (145.0 U/g) for chitinase activity. It could be speculated that the BTL-11@NSCS NPs could destroy the cell wall structure of *R. solani* by inducing the hydrolysis of chitin in the cell wall to produce *N*-acetylglucosamine.

Impact on *R. solani* cell membrane permeability

As shown in Fig. 9B and Additional file 1: Table S4, the malondialdehyde (MDA) content of rice blast fungus

showed a significant increase with the treatment concentration of medication. The findings indicated that BTL-11 and BTL-11@NSCS NPs were highly susceptible to causing increased lipid peroxidation of *R. solani* cell membrane, destroyed the cell membrane, and then inhibited or even killed the rice blast cells.

The protein content increased with the increase of agent concentration (Fig. 9C, Additional file 1: Table S5). This may be due to the fact that when subjected to adversities such as high concentrations of BTL-11 and BTL-11@NSCS NPs, rice blast fungi could increase the cellular defense against adverse environments by enhancing their own metabolisms, and synthesizing soluble proteins ability, respectively.

The change in total sugar content showed a highly significant decreasing trend (Fig. 9D, Additional file 1: Table S6), compared to the CK, which decreased by 78.8, 81.2% at 100 $\mu\text{g}/\text{mL}$, respectively. These consequences revealed that BTL-11 and BTL-11@NSCS NPs could inhibit sugar synthesis and metabolism, reduce the ability of fungal cells to utilize nutrients and ultimately affecting the normal growth of *R. solani*.

In order to clarify the destructive effects of BTL-11 and BTL-11@NSCS NPs on the cell membrane of *R. solani* (Fig. 10), fluorescent dye staining was performed after the rice blast fungus was treated with different

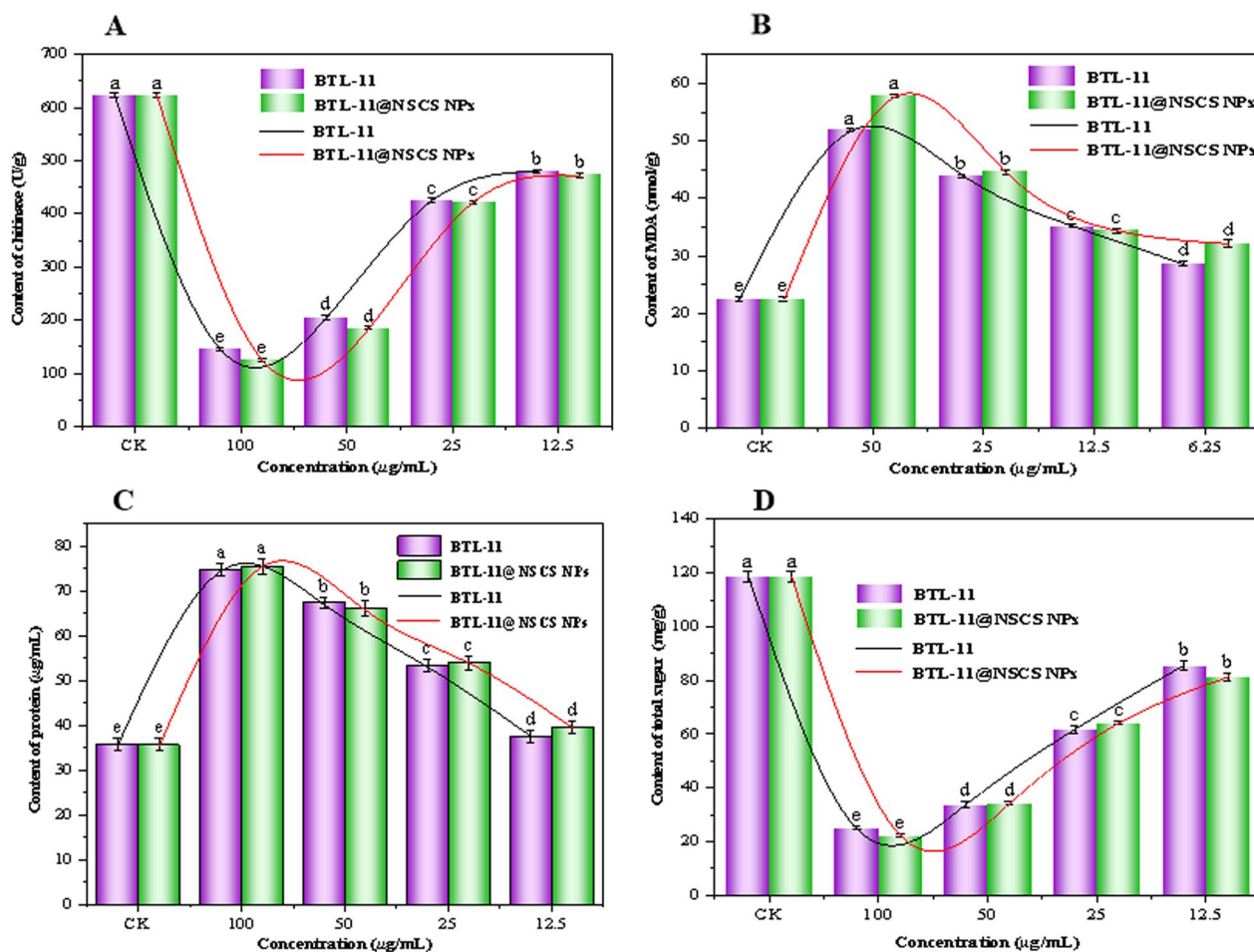


Fig. 9 Effect of different concentrations of BTL-11 and BTL-11@NSCS NPs on chitinase (A), MDA (B), protein (C), and total sugar (D) content of *R. solani*

concentrations of compounds for 12 h. The findings revealed that the morphology of mycelium was severely changed after being treated with BTL-11 (Fig. 10B, B-b) and BTL-11@NSCS NPs (Fig. 10E, E-e) at 20 μg/mL, which exhibited severe changes in mycelial morphology, with pleated hyphae, and intracellular agglutination. Whereas, the hyphae were well-grown, and a small amount of cytoplasmic unevenness of the mycorrhizal body occurred (Fig. 10C, C-c, E, F-f) at 5 μg/mL. The above results indicated that the treatment of rice blast fungus with BTL-11 and BTL-11@NSCS NPs caused cell membrane disruption and increased cell membrane permeability.

Effect on growth and respiratory energy metabolism in rice sheath blight

After being treated with different concentrations of BTL-11 and BTL-11@NSCS NPs, the mycelial volume of *R. solani* was significantly different from that of the CK, and

the inhibition rate increased with the increase of concentration (Fig. 11A, B). Those showed that BTL-11 and BTL-11@NSCS NPs could effectively enter into the intracellular to interfere with the growth of the fungus, which in turn affected the normal growth of rice blast fungus, thus achieving the effect of fungal inhibition.

In vivo trials against rice sheath blight disease

Preliminary in vitro inhibitory activity and mechanism of action experiments had demonstrated that BTL-11 and BTL-11@NSCS NPs exhibited the favorable inhibitory activity against *R. solani*, which was further explored to investigate their inhibitory activities against the pathogens in vivo. As displayed in Table 2 and Fig. 12, the protection efficiency of BTL-11 for cultivated rice leaf and sheath was 79.6 and 76.5%, respectively. By contrast, the BTL-11@NSCS NPs anti-fungal ability was strongly released and afforded significant control efficiencies of 85.9 and 81.1% at 200 μg/mL. Those effects were

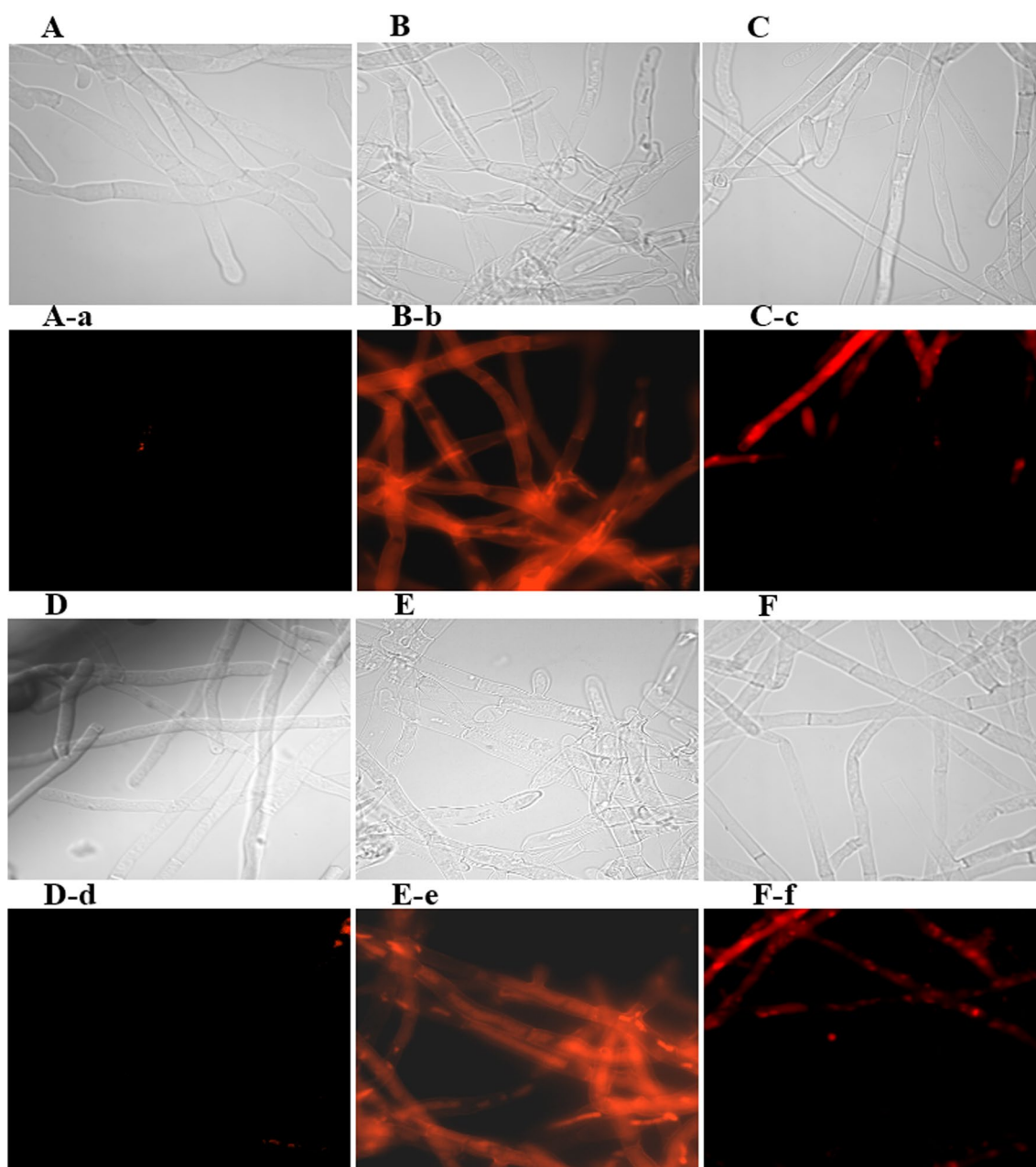


Fig. 10 Effect of BTL-11 and BTL-11@NSCS NPs on membrane integrity of *R. solani*. **A, A-a**: CK; **B, B-b**: BTL-11 (20 µg/mL); **C, C-c**: BTL-11 (5 µg/mL); **D, D-d**: CK; **E, E-e**: BTL-11@NSCS NPs (20 µg/mL); **F, F-f**: BTL-11@NSCS NPs (5 µg/mL); magnification: 100 × 10; scale for 10 µm

significantly better than those of the agricultural fungicide azoxystrobin (51.5 and 66.5%). Furthermore, the *R. solani* symptoms were distinctly alleviated from the whole perspective, manifesting that a nanoencapsulated pesticides fungicide for managing fungal infections was probably developed with improved safety.

Molecular docking of BTL-11 with oxidoreductase of *R. solani*

In the present work, the systematically structural optimizations focused on benzothiazolamide structures strikingly generated the promising candidate BTL-11 that exhibited the nonnegligible inhibitory effect against *R. solani* in vitro and in vivo. Subsequently, the molecular docking of the bioactive molecules BTL-11 and

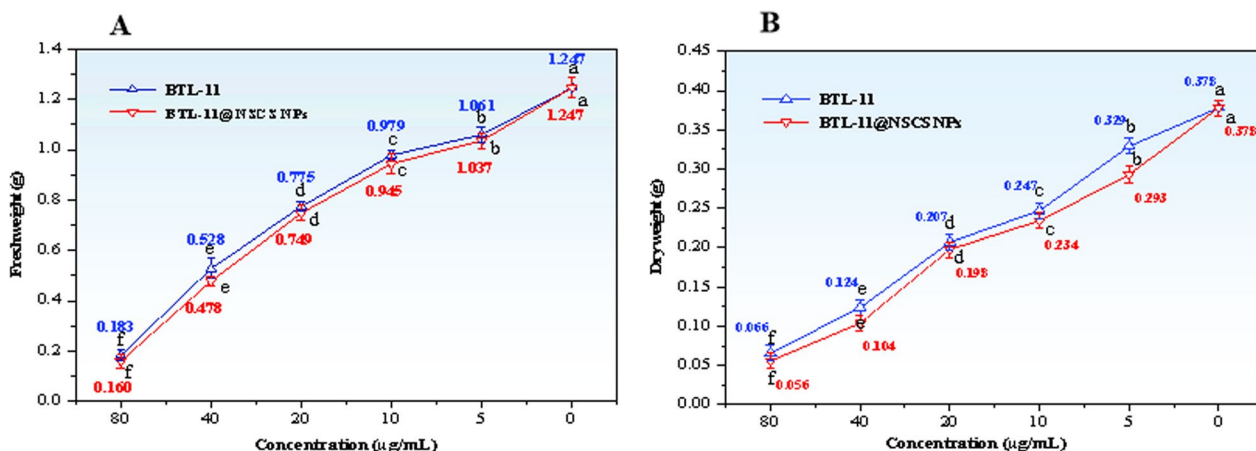


Fig. 11 Effect of BTL-11 and BTL-11@NSCS NPs on the amount of mycelial growth of *R. solani*

Table 2 In vivo protective activity against *R. solani* at 200 µg/mL^A

Treatment	leaf of rice ^B		sheath of rice ^B	
	Lesion length (mm)	Control efficacy (%)	Lesion length (mm)	Control efficacy (%)
BTL-11	8.7 ± 1.1c	79.6	10.7 ± 1.2c	76.5
BTL-11@NSCS NPs	6.0 ± 0.6d	85.9	8.6 ± 1.1d	81.1
azoxystrobin	20.7 ± 1.6b	51.5	15.3 ± 1.2b	66.5
CK	42.7 ± 1.3a	–	45.7 ± 2.3a	–

^A The experiments were repeated 3 times, *P* < 0.05

^B Values are the mean ± SD of 12 leaves

fluopyram with oxidoreductase was conducted to explore their differences in binding modes.

As can be seen from Fig. 13, the bioactive molecules BTL-11 and fluopyram were well-embedded in the active protein pocket on oxidoreductase via approximately the same conformations that roughly gave them similar interactions with most surrounding residues [61]. For example, THR 99 formed a strong hydrogen bond with the emerged as hydrogen-bond donors in BTL-11 (distance = 2.67 Å), GLY formed a hydrogen bond with the emerged as hydrogen bond donors fluopyram (distance = 2.70 Å). Concurrently, the 6-chlorobenzothiazole fragment of the title BTL-11 was linked to LEU 43 (distance = 4.93 and 5.49 Å), LEU 49 (distance = 4.35 and 5.30 Å), and HIS 98 (distance = 4.64 and 5.38 Å) residues to form multiple interactions, the trifluoromethyl pyrazole/benzene fragment of fluopyram connected with the LEU 55 (distance = 5.06 and 5.21 Å) and PHE 56 (distance = 3.66 and 4.25 Å) residues also formed multiple interactions. Among them, the HIS is one of the most

important amino acid residues within the active pocket of the oxidoreductase, and it was not present in the interaction pattern of fluoropyran. To some extent, the above mentioned similar interactions of the bioactive molecule BTL-11 and fluopyram with oxidoreductase crucial residues might be the underlying factor that maintained their anti-fungal activities against phytopathogenic microorganisms. The above molecular docking results provided an important basis for the feasibility of the designed benzothiazole amides derivatives as potential biocides substitutes.

Conclusions

Our study showed that BTL-11@NSCS NPs pesticides displayed good fluidity, solubility, and a high drug loading. In addition, the sustained release profile of BTL-11@NSCS NPs can enhance the drug's protective effectiveness. No cytotoxic effects were observed for BTL-11@NSCS NPs suggesting their safety for using in crop growth. This suggests showed that a viable polymeric nanocarrier technology that can be utilized for

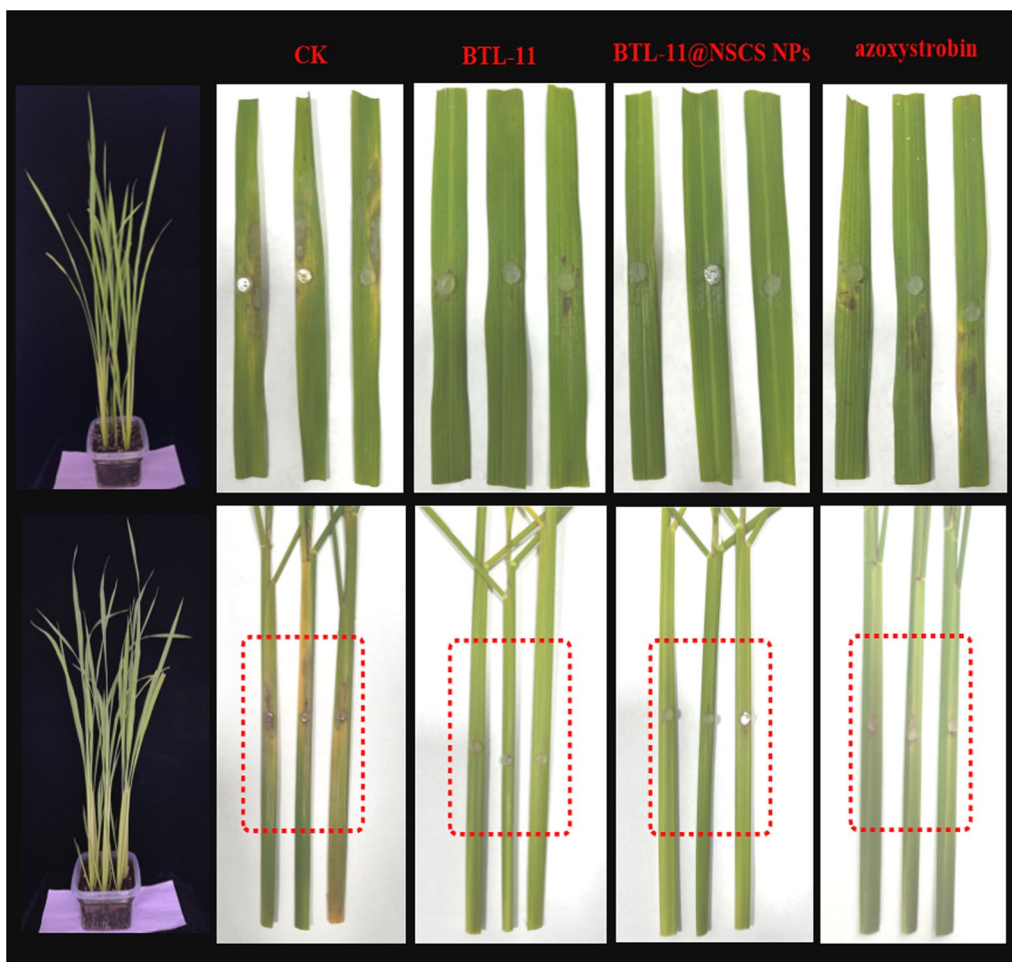


Fig. 12 In vivo protective effect of BTL-11 and BTL-11@NSCS NPs against *R. solani* using leaves and sheathes of cultivated rice at 200 µg/mL

the development of bio-compatible and safe agricultural fungicides. Notably, as depicted in Additional file 1: Table S1 and Additional file 1: Fig. S2, compared with BTL-11, BTL-11@NSCS NPs has a small, uniform, stable morphology feature, and outstanding physico-chemical properties, thereby contributing to satisfactory anti-fungal activity. The solubility bio-activity of the bioactive molecule BTL-11 was enhanced by carrier encapsulation, which solves the problem of small molecules for bio-agricultural applications to a certain extent. The mechanism of action studies suggested that BTL-11@NSCS NPs could inhibit or even kill *R. solani* cells by changing mycelial morphology, destroying the cell wall, affecting the intensification of intracellular lipid peroxidation, and influencing protein

synthesis and total sugar content, and then affecting rice sheath blight fungi lesion cells. According to a pot test on *R. solani*, BTL-11@NSCS NPs significantly reduced *R. solani* symptoms, with a control effect of 85.9% at 200 µg/mL, which was significantly better than that of azoxystrobin (51.5%). In the light of the foregoing investigations, we expected that green, safe, eco-friendly, and bio-compatible nanopesticides can be used for plant disease control.

Supplementary information

Supplementary data including Additional file 1: Table S1–S7, Additional file 1: Fig. S1–S57 and characterization of target compounds BTL-1–BTL-24.

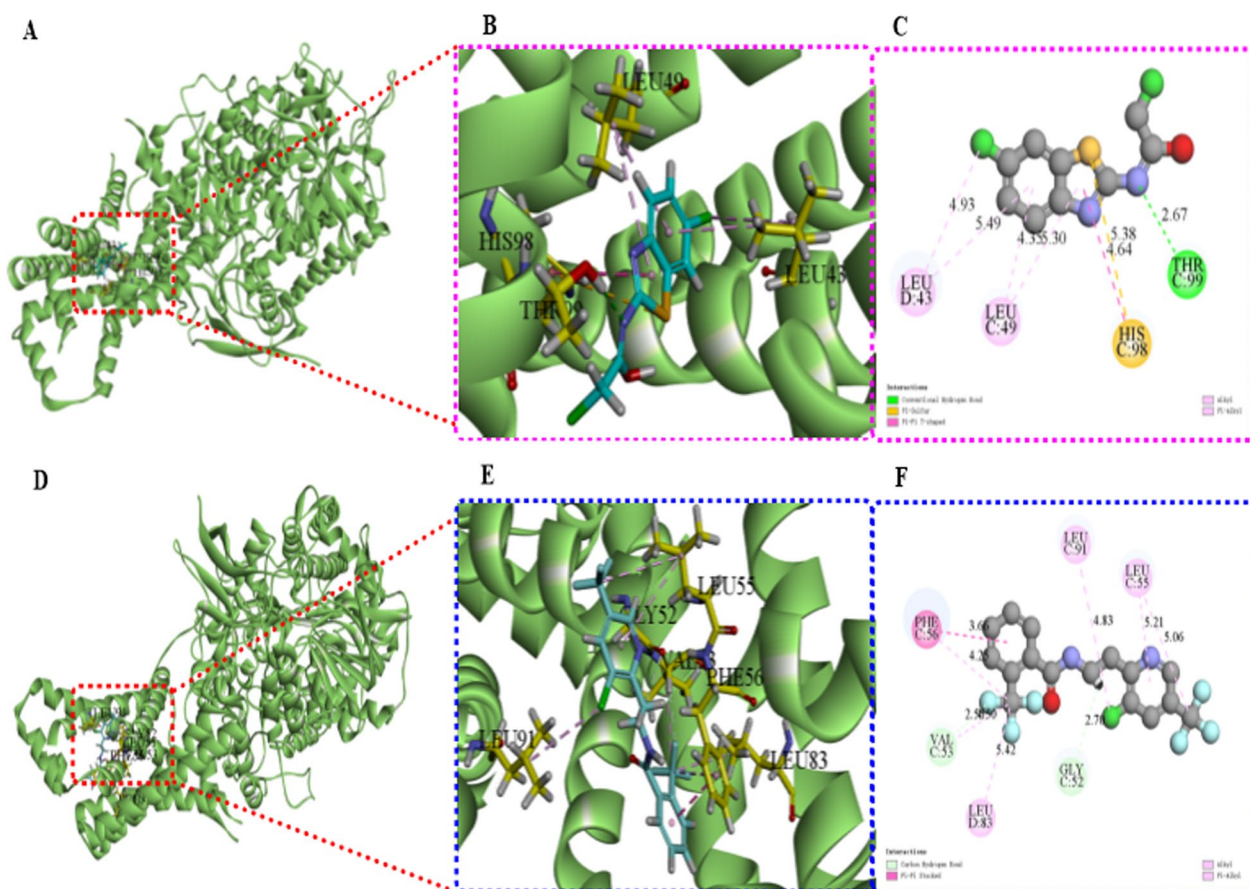


Fig. 13 Docking analyses between BTL-11 (A, B, C) or fluopyram (D, E, F) and oxidoreductase of *R. solani*

Supplementary Information

The online version contains supplementary material available at <https://doi.org/10.1186/s12951-024-02386-8>.

Additional file 1. Table S1. Loading content (LC) and encapsulation efficiency (EE)³. Table S2. In vitro activity of BTL-1–BTL-24 at 10 µg/mL against *R. solani*, *P. capsici*, *B. cinerea*, and *S. sclerotiorum*⁴. Table S3. Effect of BTL-11 and BTL-11@NSCS NPs on chitinase content of *R. solani*⁵. Table S4. Effect of BTL-11 and BTL-11@NSCS NPs on MDA content of *R. solani*⁶. Table S5. Effect of BTL-11 and BTL-11@NSCS NPs on protein content of *R. solani*⁶. Table S6. Effect of BTL-11 and BTL-11@NSCS NPs on total sugar content of *R. solani*⁶. Table S7. X-ray single crystal data of compound BTL-8. Fig. S1 Morphology of mycelia *R. solani* treated with BTL-11 and BTL-11@NSCS NPs at 20 µg/mL. A-1, A-2: CK; B-1, B-2: BTL-11; C-1, C-2: BTL-11@NSCS NPs; magnification: 10x10; scale for 10 µm. Fig. S2 Photographs of solutions of NSCS 2 mg/mL in water, BTL-11@NSCS NPs: BTL-11 2 mg/mL in NSCS solution, BTL-11 2 mg/mL in water. Fig. S3 X-ray single crystal structure of compound BTL-8. Fig. S4 ¹H NMR for compound BTL-1. Fig. S5 ¹³C NMR for compound BTL-1. Fig. S6 ¹H NMR for compound BTL-2. Fig. S7 ¹³C NMR for compound BTL-2. Fig. S8 ¹⁹F NMR for compound BTL-2. Fig. S9 ¹H NMR for compound BTL-3. Fig. S10 ¹³C NMR for compound BTL-3. Fig. S11 ¹H NMR for compound BTL-4. Fig. S12 ¹³C NMR for compound BTL-4. Fig. S13 ¹H NMR for compound BTL-5. Fig. S14 ¹³C NMR for compound BTL-5. Fig. S15 ¹H NMR for compound BTL-6. Fig. S16 ¹³C NMR for compound BTL-6. Fig. S17 ¹H NMR for compound BTL-7. Fig. S18 ¹³C NMR for compound BTL-7. Fig. S19 ¹⁹F NMR for compound BTL-7. Fig. S20 ¹H NMR for compound BTL-8. Fig. S21 ¹³C NMR for compound BTL-8. Fig. S22 ¹H NMR for compound BTL-9. Fig. S23 ¹³C NMR for compound BTL-9. Fig. S24 ¹H NMR

for compound BTL-10. Fig. S25 ¹³C NMR for compound BTL-10. Fig. S26 ¹⁹F NMR for compound BTL-10. Fig. S27 ¹H NMR for compound BTL-11. Fig. S28 ¹³C NMR for compound BTL-11. Fig. S29 ¹H NMR for compound BTL-12. Fig. S30 ¹³C NMR for compound BTL-12. Fig. S31 ¹H NMR for compound BTL-13. Fig. S32 ¹³C NMR for compound BTL-13. Fig. S33 ¹H NMR for compound BTL-14. Fig. S34 ¹³C NMR for compound BTL-14. Fig. S35 ¹H NMR for compound BTL-15. Fig. S36 ¹³C NMR for compound BTL-15. Fig. S37 ¹⁹F NMR for compound BTL-15. Fig. S38 ¹H NMR for compound BTL-16. Fig. S39 ¹³C NMR for compound BTL-16. Fig. S40 ¹H NMR for compound BTL-17. Fig. S41 ¹³C NMR for compound BTL-17. Fig. S42 ¹⁹F NMR for compound BTL-17. Fig. S43 ¹H NMR for compound BTL-18. Fig. S44 ¹³C NMR for compound BTL-18. Fig. S45 ¹H NMR for compound BTL-19. Fig. S46 ¹³C NMR for compound BTL-19. Fig. S47 ¹H NMR for compound BTL-20. Fig. S48 ¹³C NMR for compound BTL-20. Fig. S49 ¹H NMR for compound BTL-21. Fig. S50 ¹³C NMR for compound BTL-21. Fig. S51 ¹H NMR for compound BTL-22. Fig. S52 ¹³C NMR for compound BTL-22. Fig. S53 ¹⁹F NMR for compound BTL-22. Fig. S54 ¹H NMR for compound BTL-23. Fig. S55 ¹³C NMR for compound BTL-23. Fig. S56 ¹H NMR for compound BTL-24. Fig. S57 ¹³C NMR for compound BTL-24.

Acknowledgements

Not applicable.

Author contributions

The manuscript was written through contributions of all authors. All authors have given approval to the final version of the manuscript. QZ: Conceptualization, Methodology, Software, Data curation, Writing—Original draft

preparation, Writing—review and editing. ZX: Conceptualization, Methodology, Writing—Original draft preparation. YZ: Supervision, Formal analysis, Project administration. ZS: Software, Investigation. WZ: Validation. NZ: Visualization. CY: Validation. CG: Methodology. YZ: Supervision. WX: Writing—review and editing, Funding acquisition. All authors read and approved the final manuscript.

Funding

This work was supported by the National Nature Science Foundation of China (No. 32072446), the Science Foundation of Guizhou Province (No. 20192452), Science and Technology Project of Bijie City ([2023]15), Coal and Phosphorus Chemical Industry Engineering Technology Center of Bijie (2015-01), Coal Chemical Engineering 2011 Collaborative Innovation Center of Guizhou (2014-08).

Availability of data and materials

All relevant data are available with the article and its Additional file 1, or available the corresponding authors upon reasonable requests.

Declarations

Competing interests

The authors declare that they have no known competing financial interests or personal relationships that could have appeared to influence the work reported in this paper.

Consent for publication

Not applicable.

Author details

¹National Key Laboratory of Green Pesticide, Key Laboratory of Green Pesticide and Agricultural Bioengineering, Ministry of Education, Center for R&D of Fine Chemicals of Guizhou University, Guiyang 550025, China. ²College of Chemistry and Chemical Engineering, Guizhou University of Engineering Science, Bijie 551700, China.

Received: 19 January 2024 Accepted: 7 March 2024

Published online: 19 March 2024

References

- Pennisi E. Armed and dangerous. *Science*. 2010;327:804–9.
- Fisher MC, Henk DA, Briggs CJ, Brownstein JS, Madoff LC, McCraw SL. Emerging fungal threats to animal, plant and ecosystem health. *Nature*. 2012;484:186–94.
- Tuncel NY. Stabilization of rice bran: a review. *Foods*. 2023;12:12091924.
- Godfray HCJ, Mason-D'Croz D, Robinson S. Food system consequences of a fungal disease epidemic in a major crop. *Philos Trans R Soc B*. 2016;371:20150467.
- Prathi NB, Palit P, Madhu P, Balachandran SM, Madhav MS, Sundaram RM, Mangrauthia SK. Proteomic and transcriptomic approaches to identify resistance and susceptibility related proteins in contrasting rice genotypes infected with fungal pathogen *Rhizoctonia solani*. *Plant Physiol Biochem*. 2018;130:258–66.
- Miller LF, Jiranek J, Brownell M, Coffey S, Gray B, Stahl M, Metcalf CJE. Predicting the effects of climate change on the cross-scale epidemiological dynamics of a fungal plant pathogen. *Sci Rep*. 2022;12:14823–38.
- Deng YM, Tao K, Jin H, Hou TP. Mechanism of action of novel pyrazole carboxamide containing a diarylamine scaffold against *Rhizoctonia solani*. *J Agric Food Chem*. 2020;68:11068–76.
- Lv P, Chen YL, Wang DW, Wu XW, Li QX, Hua RM. Synthesis, characterization, and anti-fungal evaluation of thiolactomycin derivatives. *Engineering*. 2020;6:560–8.
- Pan T, Ye J, Li J, Gui K, Li J, Feng J, Ma Z, Lei P, Gao Y. Discovery of terpene-derived quaternary ring compounds containing an oxime moiety as potential fungicides. *J Agric Food Chem*. 2023;71:3164–72.
- Sparks TC, Lorsbach BA. Perspectives on the agrochemical industry and agrochemical discovery. *Pest Manage Sci*. 2017;73:672–8.
- Sedlak DL. The food–environment nexus. *Environ Sci Technol*. 2019;53:6597–8.
- Aliferis KA, Jabaji S. Metabolite composition and bioactivity of *Rhizoctonia solani sclerotial* exudates. *J Agric Food Chem*. 2010;58:7604–15.
- Chhipa H. Nanofertilizers and nanopesticides for agriculture. *Environ Chem Lett*. 2016;15:15–22.
- Neeraja C, Anil K, Purushotham P, Suma K, Sarma P, Moerschbacher BM, Podile AR. Biotechnological approaches to develop bacterial chitinases as a bioshield against fungal diseases of plants. *Crit Rev Biotechnol*. 2010;30:231–41.
- Mohanty SP, Hughes DP, Salathé M. Using deep learning for image-based plant disease detection. *Front Plant Sci*. 2016;7:1–10.
- Chen J, Zhang D, Zeb A, Nanehkar A. Identification of rice plant diseases using lightweight attention networks. *Expert Syst Appl*. 2021;169:114514.
- Liu Y, Sun Y, Bai Y, Cheng X, Li H, Chen X, Chen Y. Study on mechanisms of resistance to SDHI fungicide pydiflumetofen in *Fusarium fujikuroi*. *J Agric Food Chem*. 2023;71:14330–41.
- Dijksterhuis J, Van Doorn T, Samson R, Postma J. Effects of seven fungicides on non-target aquatic fungi. *Water Air Soil Pollut*. 2011;222:421–5.
- McConnell LL, Osorio C, Hofmann T. The future of agriculture and food: sustainable approaches to achieve zero hunger. *J Agric Food Chem*. 2023;71:13165–7.
- Camara MC, Campos EVR, Monteiro RA, Pereira AES, Proenca PLF, Fraceto LF. Development of stimuli-responsive nano-based pesticides: emerging opportunities for agriculture. *J Nanobiotechnol*. 2019;17:1–19.
- Kookana RS, Boxall ABA, Reeves PT, Ashauer R, Beulke S, Chaudhry Q, Cornelis G, Fernandes TF, Gan J, Kah M, Lynch I, Ranville J, Sinclair C, Spurgeon D, Tiede K, Van den Brink PJ. Nanopesticides: guiding principles for regulatory evaluation of environmental risks. *J Agric Food Chem*. 2014;62:4227–40.
- Xiang HM, Meng J, Shao WB, Zeng D, Ji J, Wang PY, Zhou X, Qi PY, Liu LW, Yang S. Plant protein-based self-assembling core–shell nanocarrier for effectively controlling plant viruses: evidence for nanoparticle delivery behavior, plant growth promotion, and plant resistance induction. *Chem Eng J*. 2023;464:142432.
- Cherian E, Dharmendirakumar M, Baskar G. Immobilization of cellulase onto MnO₂ nanoparticles for bioethanol production by enhanced hydrolysis of agricultural waste. *Chin J Catal*. 2015;36:1223–9.
- Jian YQ, Chen X, Ahmed T, Shang QH, Zhang S, Ma ZH, Yin YN. Toxicity and action mechanisms of silver nanoparticles against the mycotoxin-producing fungus *Fusarium graminearum*. *J Adv Res*. 2022;38:1–12.
- Li XW, Chen YQ, Xu JN, Lynch I, Guo ZL, Xie CJ, Zhang P. Advanced nano-pesticides: advantage and action mechanisms. *Plant Physiol Biochem*. 2023;203:108051.
- Li B, Han LG, Ma JL, Zhao MJ, Yang BH, Xu M, Gao YJ, Xu QS, Du YG. Synthesis of acylated derivatives of chitosan oligosaccharide and evaluation of their potential antifungal agents on *Fusarium oxysporum*. *Carbohydr Polym*. 2023;314:120955.
- Ilyas RA, Aisyah HA, Nordin AH, Ngadi N, Zuhri M, Asyraf M, Sapuan S, Zainudin E, Sharma S, Abrial H, Asrofi M, Syafri E, Sari N, Rafidah M, Zakaria S, Razman M, Majid N, Ramli Z, Azmi A, Bangsar S, Ibrahim R. Natural-fiber-reinforced chitosan, chitosan blends and their nanocomposites for various advanced applications. *Polym*. 2022;14:1–36.
- Tang YX, Wu S, Lin JQ, Cheng LT, Zhou J, Xie J, Huang KX, Wang XY, Yu Y, Chen ZB, Liao GJ, Li C. Nanoparticles targeted against cryptococcal pneumonia by interactions between chitosan and its peptide ligand. *Nano Lett*. 2018;18:6207–13.
- Iqbal Y, Ahmed I, Irfan MF, Chatha SAS, Zubair M, Ullah A. Recent advances in chitosan-based materials: the synthesis, modifications and biomedical applications. *Carbohydr Polym*. 2023;321:121318.
- Sun S, Zheng JQ, Liu ZJ, Huang SL, Cheng QK, Fu Y, Cai WH, Chen D, Wang D, Zhou HM, Wang YM. High-strength and recyclable pure chitosan films manufactured by an ionic liquid assisted roll-forming method. *Chem Eng J*. 2023;463:142368.
- Saberi Rish R, Vatankhah M, Hassanisaadi M, Kennedy JF. Chitosan-based nanocomposites as coatings and packaging materials for the postharvest improvement of agricultural product: a review. *Carbohydr Polym*. 2023;309:120666.

32. Fan ZQ, Wang LS, Qin YK, Li PC. Activity of chitin/chitosan/chitosan oligo-saccharide against plant pathogenic nematodes and potential modes of application in agriculture: a review. *Carbohydr Polym.* 2023;306:120592.
33. Xu JW, Guo YJ, Tang C, Qian YP, Guo CG, Wang ZN, Li LP. Hardwood vessel-inspired chitosan-based sponge with superior compressibility, superfast adsorption and remarkable recyclability for microplastics removal in water. *Chem Eng J.* 2023;475:146130.
34. Ghaffari-Bohlouli P, Alimoradi H, Freitas Siqueira Petri D, Moghassemi S, Amorim CA, Nie L, Shavandi A. Alleviating hypoxia through self-generating oxygen and hydrogen peroxide fluorinated chitosan: insights from a kinetic study. *Chem Eng J.* 2023;473:145072.
35. Chang H, Yhee JY, Jeon S, Shim MK, Yoon HY, Lee S, Kim K. In vivo toxicity evaluation of tumor targeted glycol chitosan nanoparticles in healthy mice: repeated high-dose of glycol chitosan nanoparticles potentially induce cardiotoxicity. *J Nanobiotechnol.* 2023;21:1–14.
36. Abrica-González P, Zamora-Justo JA, Sotelo-López A, Vázquez-Martínez GR, Balderas-López JA, Muñoz-Diosdado A, Ibáñez-Hernández M. Gold nanoparticles with chitosan, *n*-acylated chitosan, and chitosan oligo-saccharide as DNA carriers. *Nanoscale Res Lett.* 2019;14:1–14.
37. Chang WT, Hsieh CH, Hsieh HS, Chen C. Conversion of crude chitosan to an anti-fungal protease by *Bacillus cereus*. *World J Microbiol Biotechnol.* 2009;25:375–82.
38. Soltani SMN, Zerafat MM, Sabbaghi S. A comparative study of gelatin and starch-based nano-composite films modified by nano-cellulose and chitosan for food packaging applications. *Carbohydr Polym.* 2018;189:48–55.
39. Chakravartula SSN, Lourenço RV, Balestra F, Bittante AMQB, Sobral PJA, Rosa MD. Influence of pitanga (*Eugenia uniflora* L.) leaf extract and/or natamycin on properties of cassava starch/chitosan active films. *Food Packag Shelf Life.* 2020;24:10498.
40. Cai B, Zou Q, Zuo Y, Mei QJ, Ma JQ, Lin LL, Chen L, Li YB. Injectable gel constructs with regenerative and anti-infective dual effects based on assembled chitosan microspheres. *ACS Appl Mater Interfaces.* 2018;10:25099–112.
41. Li X, Zeng DL, Ke P, Wang GH, Zhang DK. Synthesis and characterization of magnetic chitosan microspheres for drug delivery. *RSC Adv.* 2020;10:7163–9.
42. Ren LL, Xu J, Zhang YC, Zhou J, Chen DH, Chang ZY. Preparation and characterization of porous chitosan microspheres and adsorption performance for hexavalent chromium. *Int J Biol Macromol.* 2019;135:898–906.
43. Sun Y, Yang ZH, Liu QS, Sun XB, Chen LL, Sun L, Gu W. Design, synthesis, and fungicidal evaluation of novel 1,3-benzodioxole-pyrimidine derivatives as potential succinate dehydrogenase inhibitors. *J Agric Food Chem.* 2022;70:7360–74.
44. Kumar S, Kumar A, Verma A, Mishra AK. Synthesis and docking study of some bioactive *N*-(benzo[d]thiazol-2-yl)-2-(4-(substituted)phenoxy) acetamide on cyclo-oxygenase-2 enzyme and *in vivo* analgesic activity evaluation. *Lett Drug Des Discovery.* 2021;18:396–405.
45. Luo JX, Wu P, Yu XY, Wang RZ. Preparation and solubility of *N*-succinyl-chitosan. *Food Sci Technol.* 2014;39:255–8.
46. Khalfallah A, Mazzouzi S. Synthesis and determination of critical micelle concentration of betainthioates surfactants. *J Surfactants Deterg.* 2020;10:12477.
47. Tryfon P, Kamou NN, Pavlou A, Mourdikoudis S, Menkissoglu-Spiroudi U, Dendrinou-Samara C. Nanocapsules of ZnO nanorods and geraniol as a novel mean for the effective control of *Botrytis cinerea* in tomato and cucumber plants. *Plants.* 2023;12:12051074.
48. Sahariah P, Masson M. Antimicrobial chitosan and chitosan derivatives: a review of the structure–activity relationship. *Biomacromol.* 2017;18:3846–68.
49. Dartora VFC, Passos JS, Osorio B, Hung RC, Nguyen M, Wang AJ, Panitch A. Chitosan hydrogels with MK2 inhibitor peptide-loaded nanoparticles to treat atopic dermatitis. *J Controlled Release.* 2023;362:591–605.
50. Ji QT, Hu DK, Mu XF, Tian XX, Zhou L, Yao S, Wang XH, Xiang SZ, Ye HJ, Fan LJ, Wang PY. Cucurbit[7]uril-mediated supramolecular bactericidal nanoparticles: their assembly process, controlled release, and safe treatment of intractable plant bacterial diseases. *Nano Lett.* 2022;22:4839–47.
51. Zhang J, Han RY, Ye HC, Zhou Y, Zhang ZK, Yuan EL, Feng G, Guo YX. Effect of pseudolaric acid B on biochemical and physiologic characteristics in *Colletotrichum gloeosporioides*. *Pestic Biochem Physiol.* 2017;09:75–82.
52. Song XM, Zhu XY, Li T, Liang C, Zhang M, Hu Z, Shao Y, Yang L, Tao J, Sun RF. Dehydrozingerone inspired discovery of potential broadspectrum fungicidal agents as ergosterol biosynthesis inhibitors. *J Agric Food Chem.* 2019;67:11354–63.
53. Yan W, Wang X, Li K, Li TX, Wang JJ, Yao KC. Design, synthesis, and antifungal activity of carboxamide derivatives possessing 1,2,3-triazole as potential succinate dehydrogenase inhibitors. *Pestic Biochem Physiol.* 2019;156:160–9.
54. Wang XB, Wang MQ, Han L, Jin F, Jiao J, Chen M, Yang CL, Xue W. Novel pyrazole-4-acetohydrazide derivatives potentially targeting fungal succinate dehydrogenase: design, synthesis, three-dimensional quantitative structure–activity relationship, and molecular docking. *J Agric Food Chem.* 2021;69:9557–70.
55. Yin XD, Ma KY, Wang YL, Sun Y, Shang XF, Zhao ZM, Wang RX, Chen YJ, Zhu JK, Liu YQ. Design, synthesis, and antifungal evaluation of 8-hydroxyquinoline metal complexes against phytopathogenic fungi. *J Agric Food Chem.* 2020;68:11096–104.
56. Zhou Q, Tang XM, Chen S, Zhan WL, Hu D, Zhou R, Sun N, Wu YJ, Xue W. Design, synthesis and antifungal activity of novel chalcone derivatives containing piperazine fragment. *J Agric Food Chem.* 2022;70:1029–36.
57. Xu B, Chen W, Wu ZM, Long Y, Li KT. A novel and effective *Streptomyces* sp. N2 against various phytopathogenic fungi. *Appl Biochem Biotechnol.* 2015;177:1338–47.
58. Zhang SW, Wu ZM, Yang Y, Li KT. Antifungal action of antifungal mycin N2 against *Rhizoctonia solani* by disrupting cell membrane and inhibiting succinate dehydrogenase. *Curr Microbiol.* 2020;77:254–60.
59. Tosi S, Kostadinova N, Krumova E, Pashova S, Dishliiska V, Spassova B, Vassilev S, Angelova M. Antioxidant enzyme activity of filamentous fungi isolated from Livingston island, maritime antarctica. *Polar Biol.* 2010;33:1227–37.
60. Guo X, Chen J, Gao M, Li D. An aminobutyric acid transaminase in zea mays interacts with *Rhizoctonia solani* cellulase to participate in disease resistance. *Front Plant Sci.* 2022;13:860170.
61. Wang XB, Wang A, Qiu LL, Chen M, Lu AM, Li GH, Yang CL, Xue W. Expedient discovery for novel antifungal leads targeting succinate dehydrogenase: pyrazole-4-formylhydrazide derivatives bearing a diphenyl ether fragment. *J Agric Food Chem.* 2020;68:14426–37.
62. Christou C, Agapiou A, Kokkinofa R. Use of FTIR spectroscopy and chemometrics for the classification of carobs origin. *J Adv Res.* 2018;10:1–8.
63. Urnao R, Pantelopulos GA, Straub JE. Aerosol-OT surfactant forms stable reverse micelles in apolar solvent in the absence of water. *J Phys Chem B.* 2019;123:2546–57.
64. Sharma D, Singh J. Chitosan polymer and their nanomicelles for nonviral gene delivery applications. *Bioconjugate Chem.* 2017;28:2772–83.
65. Sultana AA, Rahman MH, Joy MTR, Rana S, Khan JM, Kumar D, Ahmad A, Hoque MA, Rahman MM, Kabir SE. Interaction of sodium alginate biopolymer with sodium dodecyl sulfate in aqueous medium and different additive solutions at several temperatures. *Chem Eng Comm.* 2023;97:1–16.

Publisher's Note

Springer Nature remains neutral with regard to jurisdictional claims in published maps and institutional affiliations.